Title

Scalable Multi-Sample Single-Cell Data Analysis by Partition-Assisted Clustering and Multiple Alignments of Networks

Authors

Ye Henry Li[a,*], Dangna Li[b,*], Nikolay Samusik[c], Xiaowei Wang[d], Leying Guan[d], Garry P. Nolan[c], Wing Hung Wong[d,e,1]

*Equal Contribution: Y.H.L and D.L.

[1]To whom correspondence should be addressed. Email: whwong@stanford.edu

Author Affiliations

Ye Henry Li

[a]Structural Biology Department and Public Policy Program, Stanford University, Stanford, USA.

Dangna Li

[b]Institute for Computational and Mathematical Engineering, Stanford University, Stanford, USA.

Nikolay Samusik

[c]Department of Microbiology and Immunology, Baxter Laboratory, Stanford University, Stanford, USA

Garry P. Nolan

[c]Department of Microbiology and Immunology, Baxter Laboratory, Stanford University, Stanford, USA

Xiaowei Wang

[d]Statistics Department, Stanford University, Stanford, USA.

Leying Guan

[d]Statistics Department, Stanford University, Stanford, USA.

Wing Hung Wong

[d]Statistics Department, Stanford University, Stanford, USA.

[e]Department of Biomedical Data Science, Stanford University, Stanford, USA

Contributions

Y.H.L. and W.H.W. conceived the project. Y.H.L., D.L., L.G. and W.H.W. designed the data analysis pipeline; Y.H.L. and D.L. implemented the data analysis pipeline. N.S. generated the hand-gated CyTOF data. Y.H.L., D.L., N.S., and X.W. analyzed the data. Y.H.L., D.L., N.S. and W.H.W. wrote the manuscript and developed the figures. G.P.N and W.H.W. supervised the study.

Conflict of Interest

The authors declare no conflict of interest.

Abstract

Mass cytometry (CyTOF) has greatly expanded the capability of cytometry. It is now easy to generate multiple CyTOF datasets in a single study, with each dataset containing single-cell measurement on 50 markers for hundreds of thousands cells. Current methods do not adequately address the issues concerning combining multiple samples for subpopulation discovery, and these issues can be quickly and dramatically amplified with increasing number of samples. To overcome this limitation, we developed Partition-Assisted Clustering and Multiple Alignments of Networks (PAC-MAN) for the fast identification of cell populations in CyTOF data closely matching that of expert manual-discovery, and for alignments between subpopulations across samples to define dataset-level cellular states. PAC-MAN is computationally efficient, allowing the management of very large CyTOF datasets, which are increasingly common in clinical studies and cancer studies that monitor various tissue samples for each subject.

Introduction

Analyses of CyTOF data rely on many of the tools and ideas from flow cytometry (FC) data analysis, as CyTOF datasets are essentially higher dimensional versions of flow cytometry datasets. Currently, the most widely used method in FC is still human hand-gating, as other methods often fail to extract meaningful subpopulations of cells automatically. In hand-gating, we draw polygons or other enclosures around pockets of cell events on a two-dimensional scatterplot to define subpopulations and cellular states that are observed in the data. This process is painfully time-consuming and requires advance knowledge of the marker panel design, the quality of the staining reagents, and, most importantly, *a priori* what cell subpopulations to expect to occur in the data. When presented with a new set of marker panels and biological system, the researcher would find it difficult to delineate the cell events, especially in high-dimensional and multiple-sample datasets.

The inefficient nature of hand-gating in flow cytometry motivated algorithmic development in automatic gating. Perhaps the most popular is flowMeans(1), which is optimized for FC and can learn subpopulations in FC data(2) in an automated manner; however, it has not been successfully applied to CyTOF data analysis. Currently, most data analysis tools created for flow cytometry data analyses are not easily applicable for high-dimensional datasets(3). An exception is SPADE, which was developed and optimized specifically for the analysis of CyTOF datasets(3). flowMeans and SPADE constitute the leading computation methods in cytometry, but as shown later in this work, their performance may become sub-optimal when challenged with large and high-dimensional cytometry data sets. There are also other recent clustering-based tools that utilize dimensionality reduction and projections of high-dimensional data, however, these tools do not directly learn the subpopulations for all the cell events, and may be too slow to complete data analysis for an increasing amount of samples.

In this study, we address the data analysis challenges in two major steps. First, we propose the partition-assisted clustering (PAC) approach, which produces a partition of the k-dimensional space (k=number of markers) that captures the essential characteristic of the data distribution. This partitioning methodology is grounded in a strong mathematical framework of partition-based high-dimensional density estimation(4–8). The mathematical framework offers the guarantee that these partitions approximate the

underlying empirical data distribution; this step is faster than the recent k-nearest neighbor-based method (9) and is essential to the scalability of our clustering approach to analyze datasets with many samples. The clustering of cells based on recursive partitioning is then refined by a small number of k-means style iterations before a merging step to produce the final clustering.

Secondly, the subpopulations learned separately in multiple different but related datasets can be aligned by marker network structures (multiple alignments of networks, or MAN), making it possible to characterize the relationships of subpopulations across different samples or related datasets. The ability to do so is critical for monitoring changes in a subpopulation across different conditions. Importantly, in every study, batch effect is present; batch effects shift subpopulation signals so that the means can be different from experiment to experiment. PAC-MAN naturally addresses batch effects in finding the alignments of the same or closely related subpopulations from different samples.

PAC-MAN finds homogeneous clusters efficiently with all data points in a scalable fashion and enables the matching of these clusters across different samples to discover cluster relationships in the form of clades.

Results and Discussion

PAC

PAC has two parts: partitioning and post-processing. In the partitioning part of PAC, the data space is recursively divided into smaller hyper-rectangles based on the number of data points in the locality (Figure 1a). The partitioning is accomplished by either Bayesian Sequential Partition (BSP) with limited look-ahead (Figure 1a and 1b) or Discrepancy Sequential Partition (DSP) (Figure 1a); these are two fast variants of partition-based density estimation methods previously developed by our group (4–8), with DSP being the fastest. BSP and DSP divide the sample space into hyper-rectangles with uniform density value in each of them. The subsetting of cells according to the partitioning provides a principled way of clustering the cells that reflects the characteristics of the underlying distribution. In particular, each significant mode is captured by a number of closely located rectangles with high-density values (Figure 1c). Although this method allows a fast and unbiased localization of the high-density regions of the data space, we should not use the hyper-rectangles directly to define the final cluster boundaries for two reasons. First, real clusters are likely to be shaped elliptically, therefore, the data points in the corners of a hyper-rectangle are likely to be incorrectly clustered. Second, a real cluster is often split into more than one closely located high-density rectangles. We designed post-processing steps to overcome these limitations: 1) a small number of k-means iterations is used to round out the corners of the hyper-rectangles, 2) a merging process is implemented to ameliorate the splitting problem, which is inspired by the flowMeans algorithm. The details of post-processing are given in Materials and Methods. The resulting method is named b-PAC or d-PAC depending on whether the partition is produced by BSP or DSP.

MAN

An approach to analyze multiple related samples of CyTOF data is to pool all samples into a combined sample before detection of subpopulations. This is a natural approach under the assumptions that there are no significant batch effects or systematic shifts in cell subpopulations across the different samples. However, such assumptions may not hold due to one or more of the following reasons:

1) Dataset size and instruments used. Large number of samples usually means the samples were collected on different days with different experimental preparations. Many steps can introduce significant shifts in measurement levels.
2) Staining reagents. Reagents such as antibodies, purchased from different vendors and batch preparations can affect the overall signal. While saturation of reagents in the protocol could help eliminate the batch effects in the staining procedure, this approach is costly and might not work for all antibodies, especially those with poor specificity.
3) Normalization beads stock. While normalization beads(10) help to control for the signal level, especially within one experiment, the age of the beads stock and their preparation could lead to significant batch effects. In addition, there are different types of normalization beads and normalization calculations.
4) Human work variation. While many researchers are studying the same system (e.g., immune system), different protocols and implementation by different researchers, who sometimes perform experimental steps slightly differently, can lead to batch effects.
5) Subpopulation dynamics. The subpopulation centers can move from sample to sample due to treatments on the cells in treatment-control studies or perturbation studies. General practice is to cluster by phenotypic markers.
6) Sample background. If the data came from different cell lines or individuals in a clinical study, the measurement levels and proportions of cell subpopulations would be expected to change from sample to sample. Without expert scrutiny, it would be difficult to make sense of the data with current data analysis tools.

Could we extract shared information that allows us to interpret cross-sample similarities and differences? To ameliorate these difficulties, we have designed an alternative approach that is effective in the presence of substantial systematic between-sample variation. In this approach, each sample is analyzed separately (by PAC) to discover within-sample subpopulations. Over-partitioning in this step is allowed in order not to miss small subpopulations. The subpopulations from all samples are then compared to each other based on a pairwise dissimilarity measure designed to capture the differences in within-sample distributions (among the markers) across two subpopulations. Using this dissimilarity, we perform bottom-up hierarchical clustering of the subpopulations to represent the relationship among the subpopulations. The resulting tree of subpopulations is then used to guide the merging of subpopulations from the same sample, and to establish linkage of related subpopulations from different samples. We note that the design of a dissimilarity measure (Materials and Method) that is not sensitive to systematic sample-to-sample variation is a novel aspect of our approach. The merging of subpopulations from the same sample is also important, as it offers a way to correct any over-partitioning that may have occurred during the initial PAC analysis of each sample. We emphasize that, as with the usage of all statistical methods, the user must utilize samples or datasets that are considered as good as possible; interpretation of the analysis results rely on the researchers to collect data with validated reagents for all samples.

Rational initialization for PAC increases clustering effectiveness

Appropriate initialization of clustering is very important for eventually finding the optimal clustering labels; PAC works well because the implicit density estimation procedure yields rational centers to learn the modes of sample subpopulations. When tested on the hand-gated CyTOF data on the bone marrow sample in (14), compared to k-means alone, PAC gives lower total sums of squares and higher F-measures in the subpopulations (Figure 1d and 1e). This process also helps PAC to converge in 50 iterations (Figure 1f) in post-processing, whereas k-means performs very poorly even after 5000 iterations (Figure 1g). Through the lens of t-sne plots (Figure 1g), the PAC results are more similar to the hand-gating results, while the k-means, flowMeans, and SPADE clustering results perform poorly. In flowMeans, several large subpopulations are merged. SPADE's separation of points is inconsistent and highly heterogeneous, probably due to its down-sampling nature. On the other hand, by inspection, PAC obtains similar separation for both the major and minor subpopulations as the hand-gating results.

PAC is consistently better than flowMeans and SPADE for simulated datasets and hand-gated cytometry datasets

In the systematic simulation study, we challenged the methods with different datasets with varying number of dimensions, number of subpopulations, and separation between the subpopulations. The F-measure and p-measures for the PAC methods are consistently equal or higher than that of flowMeans and SPADE (Table 1 and Supporting Figure 2a). In addition, we observe that flowMeans gives inconsistent F-measures for similar datasets (Table 1), which may be due to the convergence of k-means to a local minimum without a rational initialization.

Next, we tested the methods based on published hand-gated cytometry datasets to see how similar the estimated subpopulations are to those obtained by human experts. We applied the methods on the hematopoietic stem cell transplant and Normal Donors datasets from the FlowCAP challenges(2) and on the subset of gated mouse bone marrow CyTOF dataset (Dataset 5) recently published(11). The gating strategy of the CyTOF dataset is provided in Supporting Figure 1. The dataset and expert gating strategy are the same as described earlier(12). Note that in the flow cytometry data, the computed F-measures are slightly lower than that reported in FlowCAP; this is due to the difference in the definition of F-measures. Overall, the PAC outperforms flowMeans and SPADE by consistently obtaining higher F-measures (Table 1). In particular, in the CyTOF data example, PAC generated significantly higher F-measures (greater than 0.82) than flowMeans and SPADE (0.59 and 0.53, respectively). In addition, PAC gives higher overall subpopulation-specific purities (Supporting Figure 2b and Supporting Table 1). These results indicate that PAC gives consistently good results for both low and high-dimensional datasets. Furthermore, PAC results match human hand-gating results very well. The consistency between PAC-MAN results and hand-gating results in this large data set confirms the practical utility of the methodology.

Separate-then-combine outperforms Pool Approach when Batch Effect is present

213 It is natural to analyze samples separately then combine the subpopulation features for downstream
214 analysis in the multiple samples setting. However, we need to resolve the batch effects.
215 Two distinct subpopulations could overlap in the combined/pooled sample, such as in the case when the
216 data came from two generations of CyTOF instruments (newer instrument elevates the signals). On the
217 other hand, in cases with changing means, two subpopulations can evolve together such that their means
218 change slightly, but enough to shadow each other when samples are merged prior to clustering.

219 First, we consider the overlapping scenario (Figure 2b). When viewed together in the merged sample, the
220 right subpopulation from sample 1 overlaps with the left subpopulation in sample 2 (Figure 2c). There is
221 no way to use expression level alone to delineate the two overlapping subpopulations (Figure 2d). By
222 learning more subpopulations using PAC, there are some hints that multiple subpopulations are present
223 (Figure 2e). Despite these hints, it would not be possible to say whether the shadowed subpopulations
224 relate in any way to other distinct subpopulations.

225 PAC-MAN resolves the overlapping issue by analyzing the samples separately (Figure 2f). Considering
226 the case in which we do not know *a priori* the number of true subpopulations, we learn three
227 subpopulations per sample. The network structures of the subpopulations discovered are presented in
228 Figure 2g and we see that the third subpopulations from the two samples share the same network
229 structures, while the first subpopulations of the two samples differ by only one edge; these respective
230 networks are clustered together in the dendrogram (Figure 2h, bottom panel). By utilizing the gene
231 networks, the clades that represent the same and/or similar subpopulations of cells can be established.
232 Clustering by network structures alone resolves the majority of points in the data (Figure 2h, top panel).
233 Furthermore, as discussed next, by incorporating marker levels into the alignment process, all the points
234 can be resolved (Figure 2i).

235 Next we consider the case with dynamic evolution of subpopulations that models the treatment-control
236 and perturbation studies. The interesting information is in tracking how subpopulations change over the
237 course of the experiment. In the simulation, we have generated two subpopulations that nearly converge
238 in mean expression profile over the time course (Figure 3a). The researcher could lose the dynamic
239 information if they were to combine the samples for clustering analysis. As in the previous case, we could
240 use PAC to learn several subpopulations per sample (Figure 3b). Then, with the assumption that there are
241 two evolving clusters from data exploration, we align the subpopulations to construct clades of same
242 and/or similar subpopulations (Figure 3c) based on the network structural information (Supporting Figure
243 3). With network and expression level information in the alignment process, the two subpopulations or
244 clades can be resolved naturally (Figure 3c).

245

246 *Network and expression alignment is better than network or expression alignment alone*

247 With networks in hand, we could further characterize the relationships between subpopulations across
248 samples. However, the alignment process needs to work well for true linkage to be established. We could
249 align by network alone, by expression (or marker) means, or both. Figures 2h, 2i, and 3c present these
250 alternatives in comparison. By using all the subpopulation networks, the results still contain subsets of
251 misplaced cells (Figures 2h top panel and 3c left panel). This is because small clusters of cells have noisy
252 underlying covariance structure; therefore, the networks cannot be accurately inferred. These structural

253 inaccuracies negatively impact the network clustering. The (mean) marker level approach also does not
254 work well (Figure 3c center panel) due to the subpopulation mean shifts across samples. On the other
255 hand, the sequential approach works well (Figures 2i and 3c right panel). In the sequential approach,
256 larger (>1500 in batch effect case; >1000 in dynamic case) subpopulations' networks are utilized for the
257 initially alignment process. Next, the smaller subpopulations, which have noisy covariance, are merged
258 with the closest larger, aligned subpopulations. Thus, more subpopulations could be discovered upstream
259 (in PAC), and the network alignment would work similarly as the smaller subpopulations, which could be
260 fragments of a distribution, do not impact the alignment process (Supporting Figure 4a and b). Moreover,
261 in the network inference step, unimportant edges can negatively impact the alignment process (Supporting
262 Figure 4c) in the network-alone case. Biologically, this means that edges that do not constrain or define
263 the cellular state should not be utilized in the alignment of cellular states. Effectively, the threshold placed
264 on the number of edges in the network inference controls for the importance of the edges. Thus, the
265 combined alignment approach works well and allows moderate over-saturation of cellular states to be
266 discovered in the PAC step so that no advance knowledge of the exact number of subpopulations is
267 necessary.

268

269 *PAC-MAN efficiently outputs meaningful data-level subpopulations for mouse tissue dataset*

270 We use the recently published mouse tissue dataset(11) to illustrate the multi-sample data analysis
271 pipeline. The processed dataset contains a total of more than 13 million cell events in 10 different tissue
272 samples, and 39 markers per event (Supporting Table 2). The original research results centered on
273 subpopulations discovered from hand-gating the bone marrow tissue data to find 'landmark'
274 subpopulations; the rest of the data points were clustered to the most similar landmark subpopulations.
275 While this enables the exploration of the overall landscape from the perspective of bone marrow cell
276 types, a significant amount of useful information from the data remains hidden.

277 In contrast, using d-PAC-MAN, the fastest approach by our comparison results, we can perform
278 subpopulation discovery for each sample automatically and then align the subpopulations across samples
279 to establish dataset-level cellular states. On a standard Core i7-44880 3.40GHz PC computer, the single-
280 thread data analysis process with all data points takes about one hour to complete, which is much faster
281 than alternative methods. With multi-threading and parallel processing, the data analysis procedure can be
282 completed very quickly. As mentioned earlier, PAC results for the bone marrow subsetted data from this
283 dataset matches closely to that of the hand-gated results. This accuracy provides confidence for applying
284 PAC to the rest of the dataset.

285 Figure 4 shows the t-sne plots for subpopulation discovered (top panel of each sample) and the
286 representative subpopulation established (bottom panel of each sample) for the entire dataset. In the PAC
287 discovery step, we learn 35 subpopulations per sample without advance knowledge of how many
288 subpopulations are present. This moderate over-partitioning of the data samples leads to a moderate
289 heterogeneity in the t-sne plots. Next, the networks are inferred for the larger subpopulations (with
290 number of cell events greater than 1000), and the networks are aligned for all the tissue samples. We
291 output 80 representative subpopulations or clades for the entire dataset to account for the traditional
292 immunology cellular states and sample-specific cellular states present. Within samples, the
293 subpopulations that cluster together by network structure are aggregated. The smaller subpopulations (not

involved in network alignment) are either merged to the closet larger subpopulation or establish their own sample-specific subpopulation by expression alignment; small subpopulations were clamped with larger clades by grouping the subpopulations into 5 clusters per sample based on the means (of marker signal). The representative subpopulations (90 total) follow the approximate distribution of the cell events on the t-sne plots and the aggregating effect cleans up the heterogeneities due to over-partitioning in the PAC step.

The cell type clades are the representative subpopulations for the entire dataset, and they could either be present across samples or in one sample alone. Their distribution is visualized by a heatmap (Figure 5). While the bone marrow sample contains many cell types, only a subset of them are directly aligned to cell types in other samples, which means using the bone marrow data as the reference point leaves much information unlocked in the dataset. The cell types in the blood and spleen samples have more alignments with cell types in other samples. The lymph node samples share many clades; the small intestine and colon samples also share many clades, probably due to closeness in biological function. The thymus sample has few clades shared with other samples, which may be due to its functional specificity.

PAC-MAN style analysis can be applied to align the tissue subpopulations by their means instead of network similarities (Supporting Figure 5). As done previously, representative clades (88 total) were outputted. The same aggregating effect is observed (Supporting Figure 5a), and this is due to the organization from dataset-level variation in the means. Comparing to the network alignment, the means linkage approach has slightly more subpopulations per sample; the subpopulation proportion heatmap (Supporting Figure 5b) shows more linking. Although the bone marrow sample subpopulations co-occur in the same clades slightly more with other sample subpopulations, this sample does not co-occur with many clades in the dataset. Thus, a PAC-MAN style analysis with means linkage also harvests additional information from the entire dataset.

To compare the network and means approaches with PAC-MAN, we study the F-measure and p-measure results with 88 total clades from each approach. The overall F-measure with all cell events is 0.7969 and the overall F-measure with clades assignments of PAC-discovered subpopulations is 0.3143. The two F-measure values suggest that the assignment of PAC-discovered subpopulations is more consistent for larger subpopulations.

To illustrate the assignment purities, the p-measures are computed for the following two cases. 1) Network clade assignment is the basis (network-justified), similar to the ground truth in the clustering comparisons previously; or 2) means clade assignment is the basis (means-justified) (Supporting Table 4). P-measure cutoff is set at 0.3 (to remove unreliable comparisons) to obtain purer clade assignments. In the network-justified case, PAC subpopulations with more than 0.3 in p-measure constitute 93.44 % of all cell events. In the means-justified case, PAC subpopulations with more than 0.3 in p-measure constitute 92.67 % of all cell events. Furthermore, if the p-measure cutoff were to increase to 0.5, the percentages of cells left for the network-justified and mean-justified cases are 6.25% and 75.16%, respectively. The network-justified case yields drastically lower numbers of cell events in the purer PAC subpopulations because the means approach has more heterogeneity in the linkages (defined as PAC-subpopulation participants in each shared clade with size of at least 2). In fact, the network approach has 100 linkages while the means approach has 209 linkages. Therefore, the extra linkages in the means approach would yield greater impurities in the network-justified case. The linkage plot (Supporting Figure 6a) shows that

335 the low linkages occur slightly more frequently for the network approach. One consequence is that the
336 network approach aggregates PAC subpopulations within sample more frequently; for instance, in the
337 thymus sample, the network approach yields 14 clades while the means approach yields 21 clades.

338 After aggregating, the clade sizes (with unique participants per sample) are plotted (Supporting Figure
339 6b). The network approach tends to find fewer linkages, as more clades have sizes of less than 4, while
340 the means approach has more clades than the network approach with clade sizes greater than 4. The
341 network approach is more conservative due to the additional constraints from network structures.
342 Conventionally, in the cytometry field, only the means are considered in the definition of cellular states.
343 Assuming the absence of batch and dynamic effects, the researcher could view the purer shared clade
344 assignments in the network-justified case (general agreement between constrained network approach and
345 means approach) as more reliable candidates of cross-sample relationships to investigate in future
346 experiments (Supporting Figure 6c).

347 Hence, the network alignment approach is in agreement that of the means approach, with network
348 alignment being more stringent in the establishment of linkages. The network PAC-MAN approach
349 defines cellular states with the additional information from network structures, and it has the effect of
350 constraining the number of linkages between samples while finding linkages for subpopulations that are
351 distant in their means.

352

353 *Network hubs provide natural annotations*

354 To further characterize the cell types, we annotate the clades within each sample using the top network
355 hub markers, which constrain the cellular states. The full annotation, along with mean average expression
356 profiles, is presented in Supporting Table 3. The clade information is presented in the ClusterID column.
357 The annotations for cells across different samples but within the same clades share hub markers. For
358 example, in clade 1 for the blood and bone marrow samples, the cells share the hub markers Ly6C and
359 CD11b. In the bone marrow sample, one important set of subpopulations is the hematopoietic stem cell
360 subpopulations. One such subpopulation is present as clade 18 with the annotation CD34-CD27-cKit-
361 Sca1 and is about 1.87 percent in the bone marrow sample. Clade 18 is only present in the bone marrow
362 sample, indicating that the PAC-MAN pipeline defines this as a sample-specific and coherent
363 subpopulation using dataset-level variation. The thymus contains a large subpopulation (84.07 percent)
364 that is characterized as CD5-CD4-CD43-CD3, suggesting it to be the maturing T-cell subpopulation.

365

366 **Conclusion**

367 We have presented the PAC-MAN data analysis pipeline. This pipeline was designed to remove major
368 roadblocks in the utilization of existing and future CyTOF datasets. First, we established a quick and
369 accurate clustering method that closely matches expert gating results; second, we demonstrated the
370 management of multiple samples by handling mean shifts and batch effects across samples. The
371 alignment allows researchers to find relationships between cells across samples without resorting to
372 pooling of all data points. This pipeline can be efficiently utilized to analyze large datasets of high-

dimension. PAC-MAN allows the cytometry field to harvest information from the increasing amount of CyTOF data available.

Materials and Methods

Partition-assisted clustering has two parts

1) Partitioning: a partition method (BSP(5) or DSP(7)) is used to learn N initial cluster centers from the original data.

2) Post-processing: A small number (m) of k-mean iterations is applied to the rectangle-based clusters from the partitioning, where m is a user-specified number. We used m=50 in our examples. After this k-means refinement, we merge the N clusters hierarchically until the desired number of clusters (this number is user-specified) is reached. The merging is based on a given distance metric for clusters. In the current implementation, we use the same distant metric as in flowMeans(1). That is, for two clusters X and Y, their distance $\mathrm{D}(\mathrm{X},\mathrm{Y})$ is defined as:

$$\mathrm{D}(\mathrm{X},\mathrm{Y}) = \min\{(\bar{x}-\bar{y})^T S_x^{-1}(\bar{x}-\bar{y}), (\bar{x}-\bar{y})^T S_y^{-1}(\bar{x}-\bar{y})\}$$

where $\bar{x}, \bar{y}$ are the sample mean of cluster X and Y, respectively. $\mathrm{S}_\mathrm{x}^{-1}$ is the inverse of the sample covariance matrix of cluster X. S_y^{-1} is defined similarly. In each step of the merging process, the two clusters having the smallest pairwise distance will be merged together into one cluster.

Partition Methods

There are two partition methods implemented in the comparison study: d-PAC and b-PAC. The results are similar, with d-PAC being the faster algorithm. Figure 1a illustrates this recursive process.

d-PAC is based on the discrepancy density estimation (DSP)(7). Discrepancy, which is widely used in the analysis of Quasi-Monte Carlo methods, is a metric for the uniformity of points within a rectangle. DSP partitions the density space recursively until the uniformity of points within each rectangle is higher than some pre-specified threshold. The dimension and the cut point of each partition are chosen to approximately maximize the gap in uniformity of two adjacent rectangles.

BSP + LL is an approximation inference algorithm for Bayesian sequential partitioning density estimation (BSP)(5). It borrows ideas from Limited-Look-ahead Optional Pólya Tree (LL-OPT), an approximate inference algorithm for Optional Pólya Tree(8). The original inference algorithm for BSP looks at one level ahead (i.e. looking at the possible cut points one level deeper) when computing the sampling probability for the next partition. It then uses resampling to prune away bad samples. Instead of looking at one level ahead, BSP + LL looks at h levels ahead (h > 1) when computing the sampling probabilities for the next partition and does not do resampling (Figure 1b). In other words, it compensates the loss from

not performing resampling with more accurate sampling probabilities. For simplicity, 'BSP + LL' is shortened to 'BSP' in the rest of the article.

F-measure

We use the F-measure for comparison of clustering results to ground truth (known in simulated data, or provided by hand-gating in real data). This measure is computed by regarding a clustering result as a series of decisions, one for each pair of data points. A true positive decision assigns two points that are in the same class (i.e. same class according to ground truth) to the same cluster, while a true negative decision assigns two points in different classes to different clusters. The F-measure is defined as the harmonic mean of the precision and recall. Precision P and recall R are defined as:

$P = \frac{TP}{TP+FP}$, $R = \frac{TP}{TP+FN}$, where TP is the total number of true positives, FP is the total number of false positives and FN is the total number of false negatives.

F-measure ranges from 0 to 1. The higher the measure, the more similar the estimated cluster result is to the ground truth. This definition of F-measure is different than that of FlowCAP challenge(2). The use of co-assignment of labels in this definition is a more accurate way to compute the true positives and negatives.

Purity-measure (p-measure)

Most of the existing measurements for clustering accuracy aim at measuring the overall accuracy of the entire datasets, i.e. comparing with the ground truth over all clusters. However, we are also interested in analyzing how well a clustering result matches the ground truth within a certain class. Specifically, consider a dataset D with K classes: $\{C_1, C_2, \dots, C_K\}$ and a given ground truth cluster labels g, we construct an index called the purity measure, or p-measure for short, to measure how well our clustering result matches g for each class C_i. This index is computed as follows:

1) For each class C_k, look for the cluster that has the maximum number of overlapping points with this class, denoted by L_{i_k}.

2) Define $S_1 = \frac{|C_k \cap L_{i_k}|}{|L_{i_k}|}$, $S_2 = \frac{|C_k \cap L_{i_k}|}{|C_k|}$, where $|\cdot|$ denotes the number of points in a set.

3) The final P-index for class C_k is given by: $P = \frac{2S_1S_2}{S_1+S_2}$.

If we were to match a big cluster with a small class, even though the overlapping may be large, S_1 would still be low since we have divided the score by the size of the cluster in S_1. In addition, we are interested in knowing how many points in C_k are clustered together by L_{i_k}, which is measured by S_2.

Network construction and comparison

After PAC, the discovered subpopulations typically have enough cells for the estimation of mutual information. This enables the construction of networks as the basis for cell type characterization. Computationally, it is not good to directly use the mutual information networks constructed this way to organize the subpopulations downstream. The distance measure used to characterize the networks could potentially give the same score for different network structures. Thus, it is necessary to threshold the network edges based on the strength of mutual information to filter out the noisy and miscellaneous edges. In this work, these subpopulation-specific networks are constructed using the MRNET network inference algorithm in the Parmigene (13) R package. The algorithm is based on mutual information ranking, and outputs significant edges connecting the markers. The top d edges (d is set to be 1x the number of markers in all examples) are used to define a network for the subpopulation. This process enables a careful calculation of the distance measure.

For each pair of subpopulation networks, we calculate a network distance, which is defined as follows. If G_1 and G_2 are two networks, let S be the set of shared edges and A be union of the of the edges in the two networks, then we define

$$\text{Similarity}(G_1, G_2) = \frac{|S|}{|A|}, \text{ where } |\cdot| \text{ denotes the size of a set.}$$

This is known as the Jaccard coefficient of the two graphs. The Jaccard distance, or 1- Jaccard coefficient, is then obtained. This is a representation of the dissimilarity between each pair of networks; the Jaccard dissimilarity is the measure used for the downstream hierarchical clustering.

Cross-sample linkage of subpopulations

We perform agglomerative clustering of the pool of subpopulations from all samples. This clustering procedure greedily links networks that are the closest in Jaccard dissimilarity, and yields a dendrogram describing the distance relationship between all the subpopulations. We cut the dendrogram to obtain the k clades of subpopulations. Subpopulations from the same sample and falling into the same clade are then merged into a single subpopulation (Figure 2a). This merging step has the effect of correcting the over-partitioning in the PAC step. No merging is performed for subpopulations from different samples sharing the same clade. In this way, we obtain k clades of subpopulations, with each clade containing no more than one subpopulation from each sample. We regard the subpopulations within each clade as being linked across samples.

In the above computation, only subpopulations with enough cells to define a stable covariance are used for network alignment via the Jaccard distance; the rest of the cell events from very small subpopulations are then merged with the closet clade by marker profile via distance of mean marker signals. If the small subpopulations are distant from the defined clades, then a new sample-specific clade is created for these small subpopulations.

Annotation of Subpopulations

To annotate the cellular states, we first apply PAC-MAN to learn the dataset-level subpopulation/clade labels. Next, these labels are used to learn the representative/clade networks. The top hubs (i.e. the most connected nodes) in these networks are used for annotation. This approach has biological significance in that important markers in a cellular state are often central to the underlying marker network; these important markers have many connections with other markers. If the connections were broken, the cell would be perturbed and driven to other states.

Running Published Methods

To run t-SNE (14) a dimensionality reduction visualization tool, we utilized the scripts published here (https://lvdmaaten.github.io/tsne/). Default settings were used.

To run SPADE, we first converted the simulated data to fcs format using Broad Institute's free CSVtoFCS online tool in GenePattern(15) (http://www.broadinstitute.org/cancer/software/genepattern#).

Next, we carried out the tests using the SPADE package in Bioconductor R(16) (https://bioconductor.org/packages/release/bioc/html/spade.html).

To run flowMeans, we carried out the tests using the flowMeans package in Bioconductor R(1) (https://bioconductor.org/packages/release/bioc/html/flowMeans.html).

In the comparisons, we selected only cases that work for all methods to make the tests as fair as possible.

To calculate the mutual information of the subpopulations, we use the infotheo R package (https://cran.r-project.org/web/packages/infotheo/index.html)

To run network inference, we use the mrnet algorithm in the parmigne R package (13). (https://www.bioconductor.org/packages/release/bioc/html/minet.html).

Code Availability

The PAC R package can be accessed at:

https://cran.r-project.org/web/packages/PAC/index.html

Simulated Data for Clustering Analysis

To compare the clustering methods, we generated simulated data from Gaussian Mixture Model varying dimension, the number of mixture components, mean, and covariance. The dimensions range from 5 to 39. The number of mixture components is varied along each dimension. The mean of each component was generated uniformly from a d-dimensional hypercube; we generated datasets using hypercube of different sizes, but kept all the other attributes the same. The covariance matrices were generated as AA^T,

where A is a random matrix whose elements were independently drawn from the standard normal distribution. The sizes of the simulated dataset range from 100k to 200k.

The simulated data are provided as (Datasets 1-6). Datasets 1-4 are for the PAC part. Dataset 1 contains data with 5 dimensions; Dataset 2 contains data with 10 dimensions; Datasets 3a and 3b contain data with 20 dimensions; and Datasets 4a and 4b contain data with 35 dimensions. The ground truth labels are included as separate sheets in each dataset.

When applying flowMeans, SPADE, and the PAC to the data, we preset the desired number of subpopulations to that in the data to allow for direct comparisons.

Gated Flow Cytometry Data

Two data files were downloaded from the FlowCAP challenges(2). One data file is from the Hematopoietic stem cell transplant (HSCT) data set; it has 9,936 cell events with 6 markers, and human gating found 5 subpopulations. Another data file is from the Normal Donors (ND) data set; it has 60,418 cell events with 12 markers, and human gating found 8 subpopulations. The files are the first ("001") of each dataset. These data files were all 1) compensated, meaning that the spectral overlap is accounted for, 2) transformed into linear space, and 3) pre-gated to remove irrelevant events. We used the data files without any further transformation and filtering. When applying flowMeans, SPADE, and the PAC to the data, we preset the desired number of subpopulations to that in the data to allow for direct comparisons.

Gated Mass Cytometry Data

Human gated mass cytometry data was obtained by gating for the conventional immunology cell types using the mouse bone marrow data recently published(11). The expert gating strategy is provided as Supporting Figure 1. The gated sample subset contains 64,639 cell events with 39 markers and 24 subpopulations and it is provided as Dataset 7.

To test the performance of different analysis methods, the data was first transformed using the asinh(x/5) function, which is the transformation used prior to hand-gating analysis; For SPADE analysis, we utilize the asinh(x/5) option in the SPADE commands. The post-clustering results from flowMeans, SPADE, b-PAC, and d-PAC were then subsetted using the indexes of gated cell events. These subsetted results are compared to the hand-gated results.

Simulated Data for MAN Analysis

To test the linking of subpopulations, we generated simulated data from multivariate Gaussian with preset signal levels and randomly generated positive definite covariance matrices. There are two cases, batch effect and dynamic. Each simulated sample file has five dimensions, with two of these varying in levels; these are the dimensions that are visualized. Dataset 5 contains the data for general batch effects case and

Dataset 6 contains the data for dynamic effects case. The ground truth labels are included as separate sheets in each dataset.

General batch scenario. Sample 1 represents data from an old instrument (instrument 1) while sample 2 represents data from a new instrument (instrument 2). There are two subpopulations per sample. These two subpopulations are the same, but their mean marker levels shifted higher up in sample 2 due to higher sensitivity of instrument 2 (Figure 2b). The subpopulations have different underlying relationships between the markers. In this simulated experiment, five markers were measured. Out of the five markers, two markers show significant shift, and we focus on these two dimensions by 2-dimensional scatterplots. In Figure 2b, the left subpopulation in sample 1 is the same as the left subpopulation in sample 2; the same with the right subpopulation. The same subpopulations were generated from multivariate Gaussian distributions with changing means with fixed covariance structure.

Dynamic scenario. Dynamic scenario models the treatment-control and perturbation studies. In the simulation, we have generated two subpopulations that nearly converge over the time course (Figure 3a). The researcher could lose the dynamic information if they were to combine the samples for clustering analysis. The related subpopulations were generated from multivariate Gaussian distributions with changing means with fixed covariance structure.

Raw CyTOF Data Processing

The researcher preprocesses the data to 1) normalize the values to normalization bead signals, 2) de-barcode the samples if multiple barcoded samples were stained and ran together, and 3) pre-gate to remove irrelevant cells and debris to clean up the data(10,17). Gene expressions look like log-normal distributions(18); given the lognormal nature of the values, the hyperbolic arcsine transform is applied to the data matrix to bring the measured marker levels (estimation of expression values) close to normality, while preserving all data points. Often, researchers use the asinh(x/5) transformation, and we use the same transformation for the CyTOF datasets analyzed in this study.

Mouse Tissue Data

In the Spitzer et al., 2015 dataset(11), three mouse strains were grown, and cells were collected from different tissues: thymus, spleen, small intestine, mesenteric lymph node, lung, liver, inguinal lymph node, colon, bone marrow, and blood. In each experiment, 39 expression markers were monitored. The authors used the C57BL6 mouse strain as the reference(11); the data was downloaded from Cytobank, and we performed our analysis on the reference strain.

First, all individual samples were filtered by taking the top 95% of cells based on DNA content and then the top 95% of cells based on cisplatin: DNA content allows the extraction of good-quality cells and cisplatin level (low) allows the extraction of live cells. Overall, the top 90% of cell events were extracted.

578 The filtered samples were then transformed by the hyperbolic arcsine (x/5) function, and merged as a
579 single file, which contains 13,236,927 cell events and 39 markers per event (Supporting Table 2).

580 Using PAC-MAN, we obtained 35 subpopulations in each sample then 80 clades for the entire dataset.
581 The 80 clades account for the traditional immune subpopulations and sample-specific subpopulations.
582 Small subpopulations not used in alignment are later merged into the closest clades; this is done by
583 performing hierarchical clustering with the marker signals to obtain 5 "expression" subclades per sample.
584 Subsequently, any clade with less than 10 cells is discarded. Subpopulation proportion heatmap was
585 plotted to visualize the subpopulation-specificities and relationships across the samples. Finally,
586 annotation was performed using the hub markers of each representative subpopulation in each sample.

587

588 **Acknowledgements**

589 We thank the members of Wong Lab, in particular Tung-yu Wu, Chen-yu Tseng and Kun Yang, for
590 critical feedback.

591 This research was supported by the Stanford SIGF-BioX fellowship and the T32 GM007276 grant to
592 Y.H.L. and the NIH R01GM109836, NSF-DMS1330132, and NSF-DMS1407557 grants to W.H.W.

593

594 **References**

595 1. Aghaeepour N, Nikolic R, Hoos HH, Brinkman RR. Rapid cell population identification in flow
596 cytometry data. Cytometry A. 2011 Jan 1;79A(1):6–13.

597 2. Aghaeepour N, Finak G, Consortium TF, Consortium TD, Hoos H, Mosmann TR, et al. Critical
598 assessment of automated flow cytometry data analysis techniques. Nat Methods. 2013
599 Mar;10(3):228–38.

600 3. Qiu P, Simonds EF, Bendall SC, Gibbs Jr KD, Bruggner RV, Linderman MD, et al. Extracting a
601 cellular hierarchy from high-dimensional cytometry data with SPADE. Nat Biotechnol. 2011
602 Oct;29(10):886–91.

603 4. Wong WH, Ma L. Optional Pólya tree and Bayesian inference. Ann Stat. 2010 Jun;38(3):1433–59.

604 5. Lu L, Jiang H, Wong WH. Multivariate Density Estimation by Bayesian Sequential Partitioning. J
605 Am Stat Assoc. 2013 Dec 1;108(504):1402–10.

606 6. Yang K, Wong WH. Discovering and Visualizing Hierarchy in the Data. ArXiv14034370 Stat
607 [Internet]. 2014 Mar 18 [cited 2015 Nov 27]; Available from: http://arxiv.org/abs/1403.4370

608 7. Yang K, Wong WH. Density Estimation via Adaptive Partition and Discrepancy Control.
609 ArXiv14041425 Stat [Internet]. 2014 Apr 4 [cited 2015 Nov 27]; Available from:
610 http://arxiv.org/abs/1404.1425

611 8. Jiang H, Mu JC, Yang K, Du C, Lu L, Wong WH. Computational Aspects of Optional Pólya Tree. J
612 Comput Graph Stat. 2015 Feb 13;0(ja):00–00.

613 9. Samusik N, Good Z, Spitzer MH, Davis KL, Nolan GP. Automated mapping of phenotype space
614 with single-cell data. Nat Methods. 2016 Jun;13(6):493–6.

615 10. Finck R, Simonds EF, Jager A, Krishnaswamy S, Sachs K, Fantl W, et al. Normalization of mass
616 cytometry data with bead standards. Cytometry A. 2013 May 1;83A(5):483–94.

617 11. Spitzer MH, Gherardini PF, Fragiadakis GK, Bhattacharya N, Yuan RT, Hotson AN, et al. An
618 interactive reference framework for modeling a dynamic immune system. Science. 2015 Jul
619 10;349(6244):1259425.

620 12. Samusik N, Good Z, Spitzer MH, Davis KL, Nolan GP. Automated mapping of phenotype space
621 with single-cell data. Nat Methods. 2016 Jun;13(6):493–6.

622 13. Sales G, Romualdi C. parmigene—a parallel R package for mutual information estimation and gene
623 network reconstruction. Bioinformatics. 2011 Jul 1;27(13):1876–7.

624 14. Maaten L van der, Hinton G. Visualizing Data using t-SNE. J Mach Learn Res. 2008;9(Nov):2579–
625 605.

626 15. Reich M, Liefeld T, Gould J, Lerner J, Tamayo P, Mesirov JP. GenePattern 2.0. Nat Genet. 2006
627 May;38(5):500–1.

628 16. Linderman MD, Bjornson Z, Simonds EF, Qiu P, Bruggner RV, Sheode K, et al. CytoSPADE:
629 high-performance analysis and visualization of high-dimensional cytometry data. Bioinformatics.
630 2012 Sep 15;28(18):2400–1.

631 17. Zunder ER, Finck R, Behbehani GK, Amir ED, Krishnaswamy S, Gonzalez VD, et al. Palladium-
632 based mass tag cell barcoding with a doublet-filtering scheme and single-cell deconvolution
633 algorithm. Nat Protoc. 2015 Feb;10(2):316–33.

634 18. Bengtsson M, Ståhlberg A, Rorsman P, Kubista M. Gene expression profiling in single cells from
635 the pancreatic islets of Langerhans reveals lognormal distribution of mRNA levels. Genome Res.
636 2005 Oct 1;15(10):1388–92.

637

638

Figure and Table Legends

Figure 1: PAC utilizes rational initialization for fast and accurate clustering convergence

(a) Partition-based methods estimate data density by cutting the data space into smaller rectangles. Bayesian Sequential Partition (BSP) divides the data space via binary partition in the middle of the bounded region, while that of Discrepancy Sequential Partition (DSP) occur at the location that balances the data point uniformly on both sides of the cut. The numbers denote sequential order of partitions. Since DSP adapts to the data points, it converges on the estimated density faster than BSP. (b) In the (one-step) look-ahead of version of partition, the algorithm cuts the data space for all potential cuts plus one step more (steps 2 and 3), and it finds the optimal future version (after step 3), which determines the actual cut (step 2). (c) The partitioning of simulated data space containing five subpopulations; the hyper-rectangles surround high-density areas, approximating the underlying distribution. (d-e) The rational initialization step helps PAC to outperform random initialization. The handgated CyTOF data was used. In this case, the overall sum of squares error is lower and the F-measure is higher for PAC. (f) The convergence of PAC toward the hand-gated results, or ground truth, is fast. It takes less than 50 downstream post-processing kmeans iterations for the PAC to achieve a significantly higher F-measure than the alternative methods. In contrast, flowMeans convergence is poor. (g) Visualization of clustering results with t-sne plot. The t-sne plots contain 10,000 cell events of the handgated CyTOF data with different set of labels drawn. Note that the colors are informative only within each panel. These labels are from kmeans, SPADE, flowMeans, b-PAC, and d-PAC. The subpopulation numbers for all methods were set to be the same as that of handgated results.

Figure 2: Overlapping batch effects can be resolved by PAC-MAN

(a) Schematic of MAN. Consider a deck of networks (in analogy to cards), with each "suit" representing a sample and each "rank" representing a unique network structure. The networks are aligned by similarity and organized on a dendrogram. The tree is cut (red line) at the user-specified level to output the desired *k* clades. Within each clade, the network structures are similar or the same. If the same sample has multiple networks in the same clade, then these networks are merged (black box around same cards). (b) Simulated data samples with two of the same subpopulations. The means shifted due to measurement batch effect. (c) When the samples are combined, as in the case of analyzing all samples together, two different subpopulations overlap. (d) The overlapped subpopulations cannot be distinguished by clustering. (e) PAC could be used to discover more subpopulations, however, the hints of the present of another subpopulation do not help to resolve the batch effect. (f) PAC was used to discover several subpopulations per sample without advanced knowledge of the exact number of subpopulations. (g) The networks of the subpopulations discovered in (f). Networks can be grouped by similarities to organize the subpopulations across samples; the alignment is based on Jaccard dissimilarity network structure characterization matrix; dendrogram of the hierarchical clustering results. (h) Resolution of batch effect by networks of all subpopulations discovered. (i) Resolution of batch effect first by gene networks of larger subpopulations and then by merging smaller subpopulations into the aligned clades.

Figure 3: Dynamic information can be extracted by PAC-MAN

(a) Ground truth of simulated samples. Two subpopulations, in blue color, almost converge in time by mean shifts. (b) PAC discovers several subpopulations per sample without advanced knowledge of the number of subpopulations present. (c) Comparison of PAC-MAN results between representative clades (number of clades set to 2). Using gene networks and expression information alone do not resolve the dynamic information. On the other hand, dynamic information is resolved first by gene networks of larger subpopulations and then by merging smaller subpopulations into the aligned clades.

Figure 4: Mouse tissue data analysis results visualized by t-sne plots.

Each t-sne plot was generated using 10,000 randomly drawn cell events from each mouse tissue sample. The results from PAC (top panel) and MAN (bottom panel) steps are presented as a pair. Initial PAC discovery was set to 35 subpopulations without advanced knowledge of the number of subpopulations in each sample. In MAN, 80 network clades were outputted, and the cellular states are defined by gene expression, network structure, and dataset-level variation. This composite definition naturally aggregates the initial 35 subpopulations to yield smaller number of subpopulations in less variable samples.

Figure 5: Clade proportions and annotation

Heatmap of clade proportions across the samples. Sample-specific clades have a value of 1, while shared clades have proportions spread across different samples. Physiologically similar samples share more clades.

Supporting Figure 1: Gating strategy of CyTOF data for methods comparison

Biaxial gating hierarchy for the mouse bone marrow CyTOF dataset. Gating strategy that was used to find 24 reference populations in the mouse bone marrow CyTOF data. Pre-gating step involved removal of doublets, dead cells, erythrocytes and neutrophils. Non-neutrophils population was either subject to cluster analysis by computational tools or subsequent gating. Dotted boxes represent 24 terminal gates that were selected as reference populations for the comparison analysis.

Supporting Figure 2: Subpopulation purity of simulated and real CyTOF data

(a) Subpopulation-specific purity plot of 35-dimensional simulated data with 10 subpopulations. The blue points denote the differences between the p-measures of the partition-based method (either d-PAC or b-PAC) and flowMeans, while the red points denote the p-measure differences between the partition methods and SPADE. The horizontal line at 0 means no difference between the methods. Most of the blue

712 and red points are above 0, indicating that the PAC generates purer subpopulations compared to the
713 ground truth. The two subplots are very similar, which means that d-PAC and b-PAC give very similar p-
714 measures. More precisely, the sum of differences between d-PAC and flowMeans and d-PAC and
715 SPADE are 0.85 and 1.09, respectively; and the overall difference between b-PAC and flowMeans and b-
716 PAC and SPADE are 0.84 and 1.08, respectively.

717 (b) Subpopulation-specific purity plot of the hand-gated CyTOF data. The same convention is used as in
718 (Supporting Figure 2a). Again, more blue and red points are above 0, indicating that the partition-based
719 methods generate purer subpopulations compared to the ground truth. There is a cluster of points below 0
720 occurring in the middle of the plot, suggesting that flowMeans and SPADE capture the mid-size
721 subpopulations more similar to hand-gating than the partition-based methods. More specifically,
722 flowMeans does better (p-measure difference of 0.1 or better; difference of less 0.1 is considered
723 practically no difference) with finding subpopulations of GMP, CD8 T cells, MEP, CD4 T cells
724 (compared to d-PAC), and Plasma cells, while SPADE does better with CD19+IgM- B cells, NK cells
725 (compared to d-PAC), CD8 T cells, NKT cells, Basophils, Short-Term HSC, and Plasma cells. However,
726 overall, PAC has a much better performance, as the absolute sum of points above 0 is higher than that of
727 points below 0. More precisely, the sum of differences between d-PAC and flowMeans and d-PAC and
728 SPADE are 1.21 and 1.45, respectively; and the overall difference between b-PAC and flowMeans and b-
729 PAC and SPADE are 2.06 and 2.31, respectively. The difference table is provided in Supporting Table 1.

730

731 **Supporting Figure 3: Gene Networks inferred from subpopulations in the dynamic example**
732 **simulated dataset**

733 Figure 3 introduced the dynamic example in which five samples each having 2 true subpopulations
734 capture the almost-convergence of means. Here the underlying gene network structures for the PAC
735 discovered subpopulations (three per sample) are presented.

736

737 **Supporting Figure 4: Comparison between aligning cross-sample subpopulations by gene network,**
738 **expression profile, or both**

739 (a) PAC can be used to discover more subpopulations, with the effect of more partitions from the true
740 clusters. (b) When over-partitioning is present, gene network or gene expression profile alone cannot
741 resolve the dynamic (or batch) effects due to noisy covariance for small fragments of distributions.
742 However, first aligning the larger subpopulations with more stable covariance, and thus network
743 structures, and then merge in the smaller subpopulations by expression profile resolves the effects. (c) If
744 more irrelevant edges were introduced, network alignment would fail due to the negative impact of the
745 miscellaneous edges; however, eliminating small subpopulations from the alignment step alleviates the
746 increased edge count problem.

747

748 **Supporting Figure 5: PAC-MAN style linkage by means**

749 (a) t-sne plots of mouse tissue samples colored by representative subpopulations labels from linkage by
750 means. (b) Subpopulation proportion heatmap of clades of samples from linkage by means.

751

752 **Supporting Figure 6: Comparison between network and means PAC-MAN**

753 (a) PAC-discovered subpopulations are aggregated by MAN into clades; the number of PAC
754 subpopulations/clades for the network and means PAC-MAN approaches are plotted. (b) After
755 aggregating shared clades within samples, the number of shared clades for the entire dataset is plotted for
756 the two PAC-MAN approaches. c) Using the network approach results as basis, the clades with strong
757 agreement (high p-measures) with the means PAC-MAN approach are given. The shared clades (present
758 in more than one sample) are reliable candidates for future experiment to find cross-sample relationships.

759

760 **Table 1: F-measure Comparisons of Methods on Simulated and Hand-gated Cytometry Datasets.**

761 F-measure is calculated using the original hand-gate labels and the estimated labels generated by each
762 analysis method. The true-positives are found if the methods assign the same labels to points belonging to
763 the same subpopulation in the hand-gated data. The more true-positives found, the higher the F-measure,
764 which ranges from 0 to 1, with 1 being the highest. Partition-based methods perform consistently well on
765 data ranging from 5 to 39 dimensions. In the simulations, d-PAC and b-PAC perform just as well or better
766 than flowMeans and SPADE. flowMeans gives drastically different F-measures for the cases
767 20_10_40_100k and 20_20_40_100k : 0.25386 vs. 0.92518; this large difference is likely due to the
768 random initiation of cluster centers. In the hand-gated datasets, SPADE has the worst performance.
769 Ultimately, the performance of flowMeans and SPADE deteriorate for the 39-dimensional real CyTOF
770 data, while d-PAC and b-PAC perform consistently well.

771 *Simulated data have the following convention: a_b_c_d, where a denotes the number of
772 dimensions/markers, b denotes the number of subpopulations, c denotes the size of the hypercube for data
773 generation, and d denotes the number of cells.

774 **from rounding up, not originally 1.00

775

776 **Supporting Table 1: Purity (p) Measure Differences in CyTOF Comparison**

777 p-measure differences in gated CyTOF data analysis comparison. The differences are shown for all the
778 annotated cell subpopulations, which are ordered by their sizes. Overall, the PAC methods give more
779 positive p-measures.

780

781 **Supporting Table 2: Sample Sizes in Mouse Tissue CyTOF Dataset**

782 The numbers of cells in the samples of Spitzer et al., 2015 CyTOF dataset. The data is from the C57BL6
783 mouse strain and a total of ten tissue samples are present. The raw column shows the number of cells

784 prior to filtering by DNA and cisplatin values. The final cell counts are shown in the filtered file (3rd)
785 column.

786

787 **Supporting Table 3: PAC-MAN Subpopulation Characterization Output for Mouse Tissue CyTOF**
788 **Dataset**

789 The full set of annotated results, along with mean expressions, subpopulation proportion and counts, are
790 reported.

791

792 **Supporting Table 4: Network-justified and means-justified p-measures for Alignments of PAC-**
793 **discovered Subpopulations**

794 The PAC-discovered subpopulations were mapped as clades in both the network and means PAC-MAN
795 approaches. The p-measures were calculated for the cases 1) network approach mapping as the basis and
796 2) means approach mapping as the basis. The comparison is the same in principle to the comparison of
797 labels for clustering methods. The results are ordered by p-measures.

798

Figure 1

a

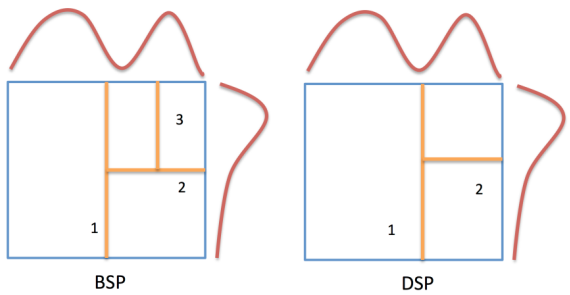

b

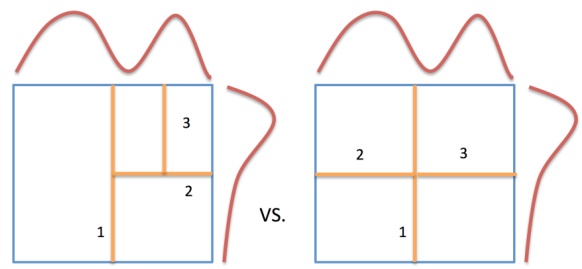

c

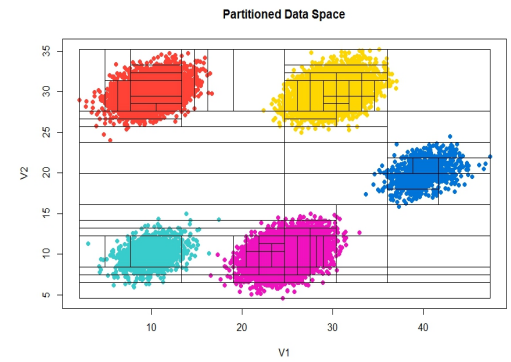

d

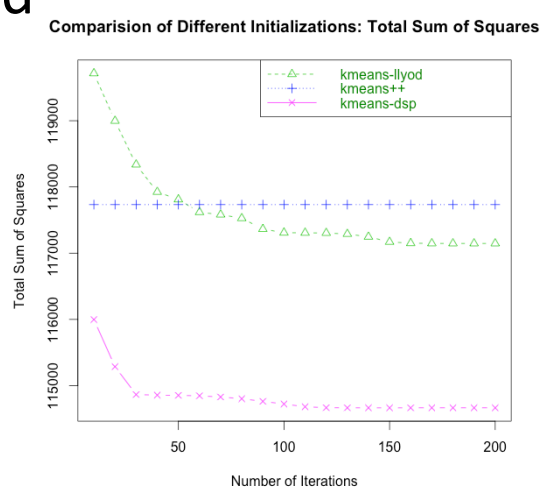

e

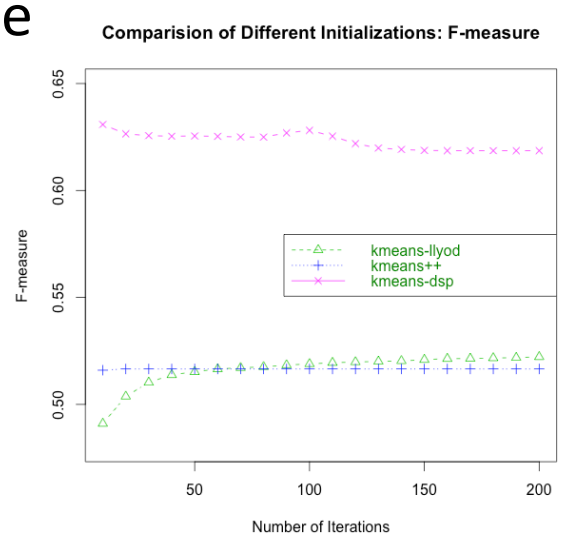

f

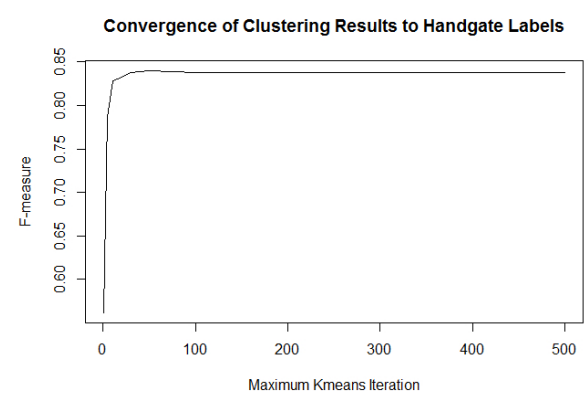

g

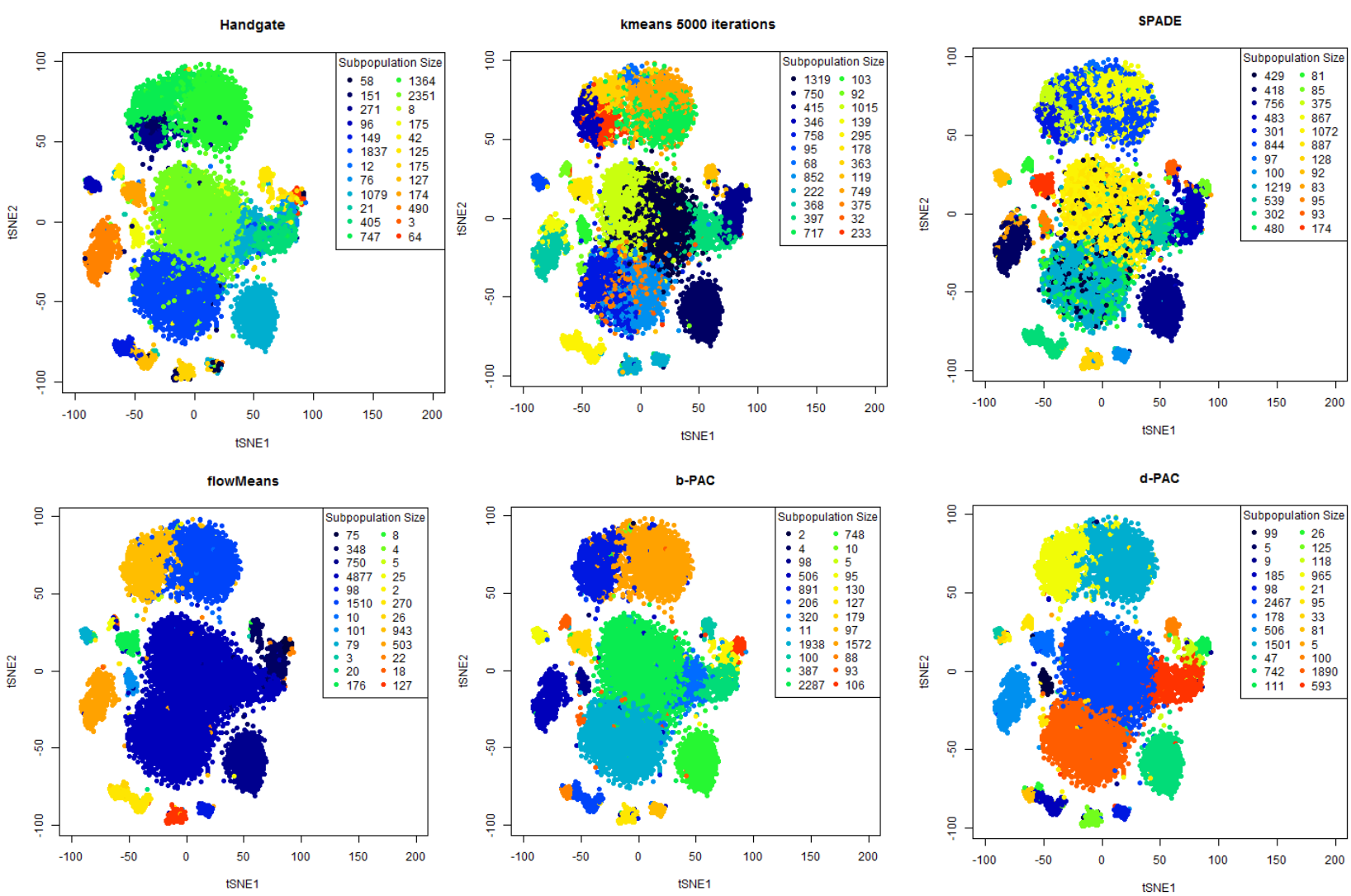

Figure 2

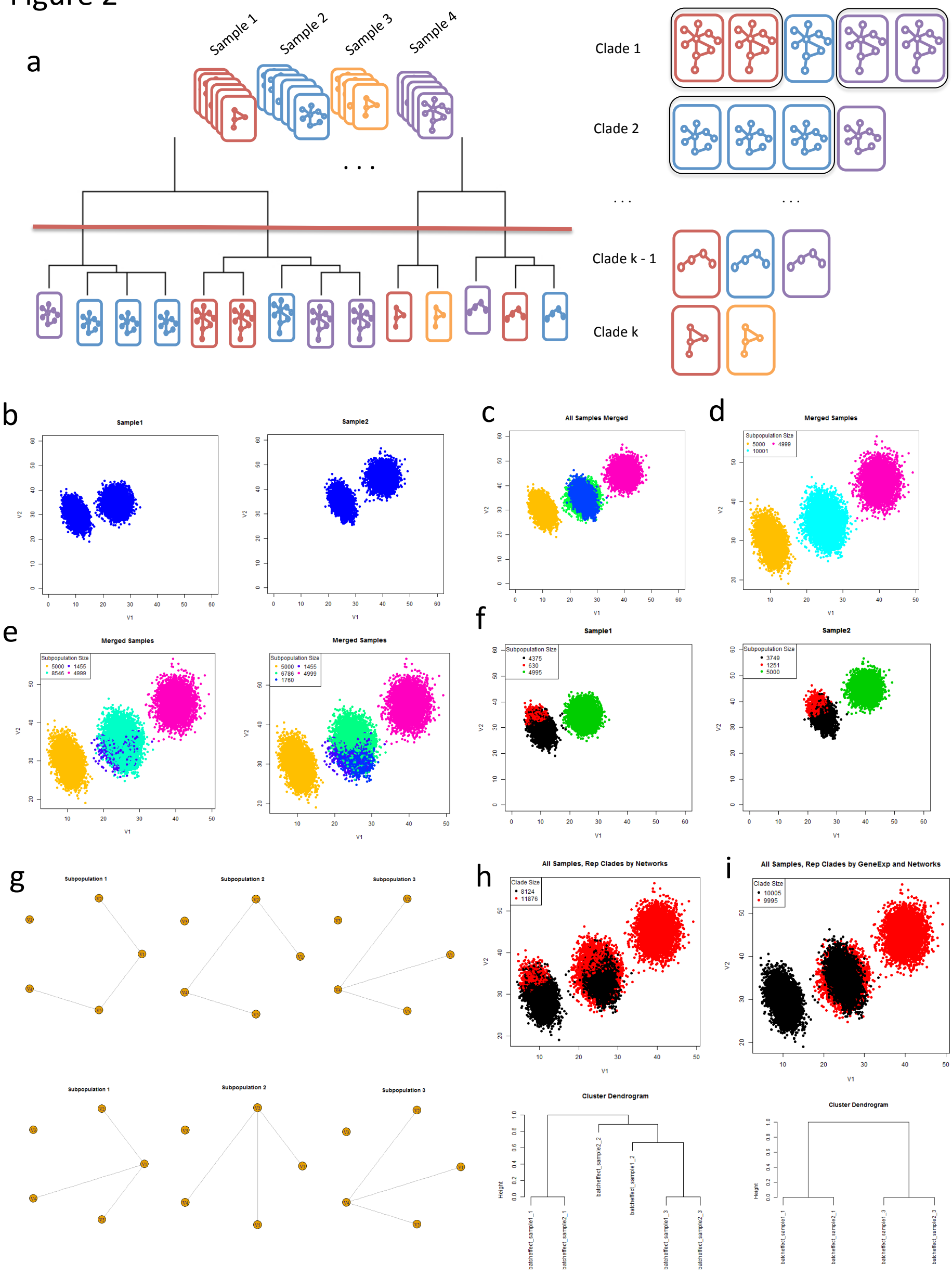
a
Sample 1
Sample 2
Sample 3
Sample 4
Clade 1
Clade 2
Clade k - 1
Clade k
b
Sample1
Sample2
c
All Samples Merged
d
Merged Samples
Subpopulation Size
5000
4999
10001
e
Merged Samples
Subpopulation Size
5000
1455
8546
4999
6786
1760
f
Sample1
Subpopulation Size
4375
630
4995
Sample2
Subpopulation Size
3749
1251
5000
g
Subpopulation 1
Subpopulation 2
Subpopulation 3
h
All Samples, Rep Clades by Networks
Clade Size
8124
11876
i
All Samples, Rep Clades by GeneExp and Networks
Clade Size
10005
9995
Cluster Dendrogram
Height
batcheffect_sample1_1
batcheffect_sample2_1
batcheffect_sample2_2
batcheffect_sample1_2
batcheffect_sample1_3
batcheffect_sample2_3
V1
V2

Figure 3

a

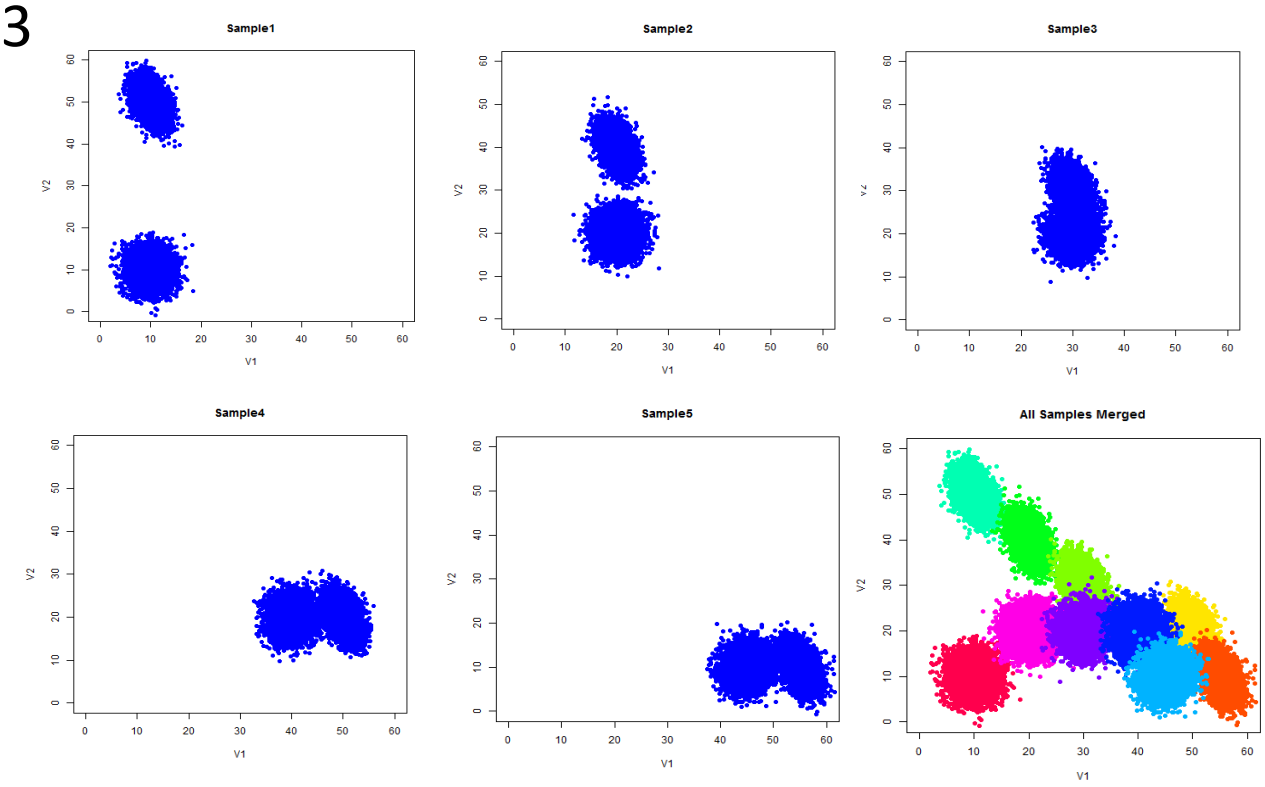
Sample1
Sample2
Sample3
Sample4
Sample5
All Samples Merged
V1
V2

b

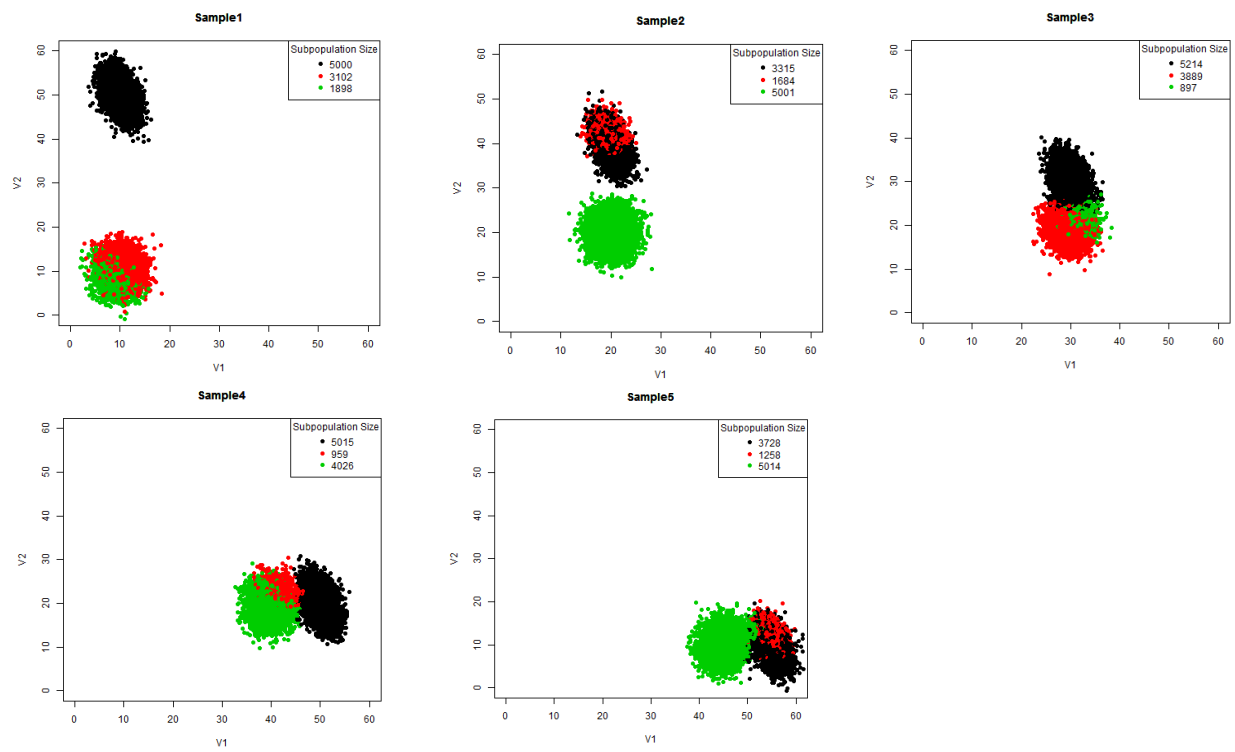
Sample1
Subpopulation Size
5000
3102
1898
Sample2
Subpopulation Size
3315
1684
5001
Sample3
Subpopulation Size
5214
3889
897
Sample4
Subpopulation Size
5015
959
4026
Sample5
Subpopulation Size
3728
1258
5014
V1
V2

c

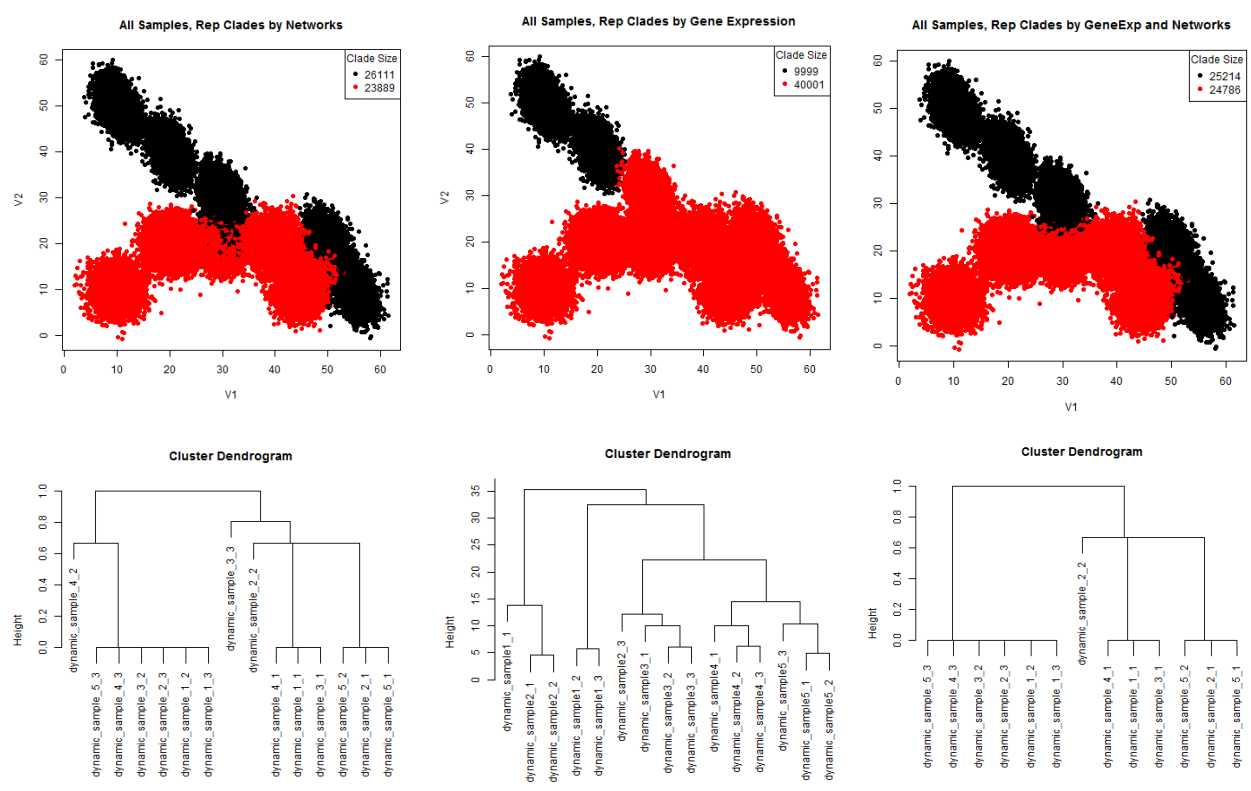
All Samples, Rep Clades by Networks
Clade Size
26111
23889
All Samples, Rep Clades by Gene Expression
Clade Size
9999
40001
All Samples, Rep Clades by GeneExp and Networks
Clade Size
25214
24786
Cluster Dendrogram
Cluster Dendrogram
Cluster Dendrogram
Height
V1
V2

Figure 4

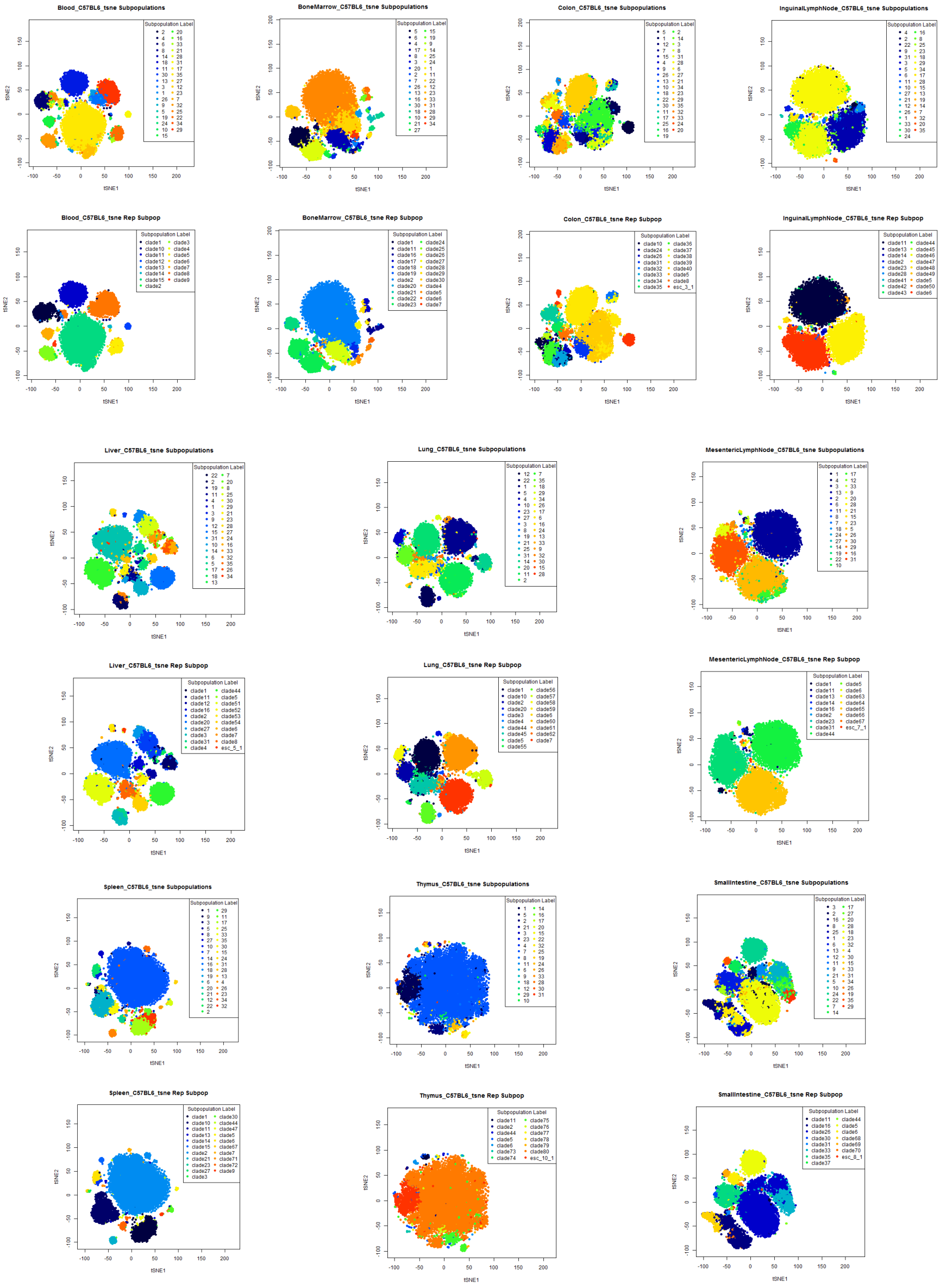
Blood_C57BL6_tsne Subpopulations
BoneMarrow_C57BL6_tsne Subpopulations
Colon_C57BL6_tsne Subpopulations
InguinalLymphNode_C57BL6_tsne Subpopulations
Blood_C57BL6_tsne Rep Subpop
BoneMarrow_C57BL6_tsne Rep Subpop
Colon_C57BL6_tsne Rep Subpop
InguinalLymphNode_C57BL6_tsne Rep Subpop
Liver_C57BL6_tsne Subpopulations
Lung_C57BL6_tsne Subpopulations
MesentericLymphNode_C57BL6_tsne Subpopulations
Liver_C57BL6_tsne Rep Subpop
Lung_C57BL6_tsne Rep Subpop
MesentericLymphNode_C57BL6_tsne Rep Subpop
Spleen_C57BL6_tsne Subpopulations
Thymus_C57BL6_tsne Subpopulations
SmallIntestine_C57BL6_tsne Subpopulations
Spleen_C57BL6_tsne Rep Subpop
Thymus_C57BL6_tsne Rep Subpop
SmallIntestine_C57BL6_tsne Rep Subpop
Subpopulation Label
tSNE1
tSNE2

Figure 5

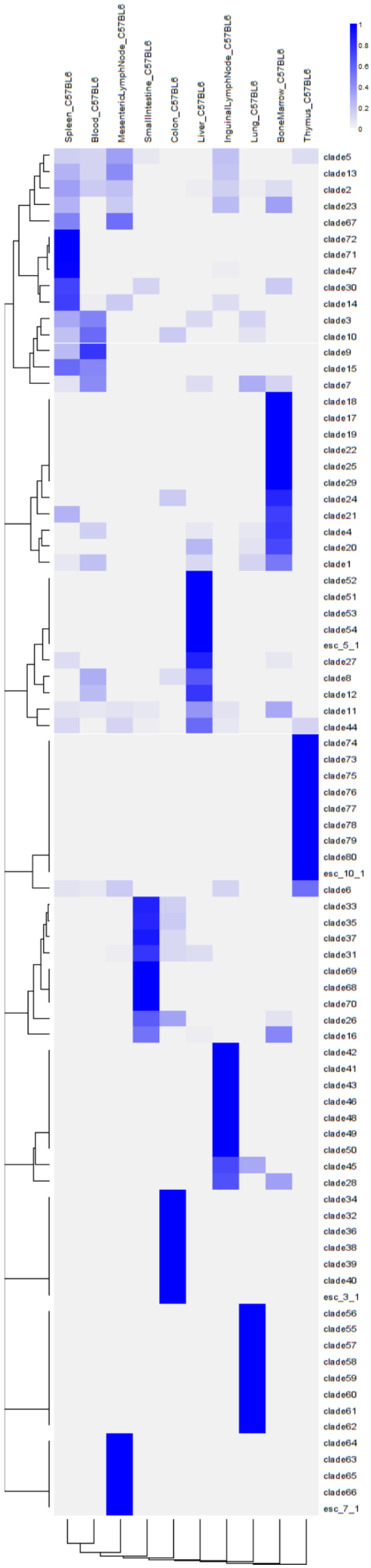
Spleen_C57BL6
Blood_C57BL6
MesentericLymphNode_C57BL6
SmallIntestine_C57BL6
Colon_C57BL6
Liver_C57BL6
InguinalLymphNode_C57BL6
Lung_C57BL6
BoneMarrow_C57BL6
Thymus_C57BL6
1
0.8
0.6
0.4
0.2
0
clade5
clade13
clade2
clade23
clade67
clade72
clade71
clade47
clade30
clade14
clade3
clade10
clade9
clade15
clade7
clade18
clade17
clade19
clade22
clade25
clade29
clade24
clade21
clade4
clade20
clade1
clade52
clade51
clade53
clade54
esc_5_1
clade27
clade8
clade12
clade11
clade44
clade74
clade73
clade75
clade76
clade77
clade78
clade79
clade80
esc_10_1
clade6
clade33
clade35
clade37
clade31
clade69
clade68
clade70
clade26
clade16
clade42
clade41
clade43
clade46
clade48
clade49
clade50
clade45
clade28
clade34
clade32
clade36
clade38
clade39
clade40
esc_3_1
clade56
clade55
clade57
clade58
clade59
clade60
clade61
clade62
clade64
clade63
clade65
clade66
esc_7_1

Supporting Figure 1

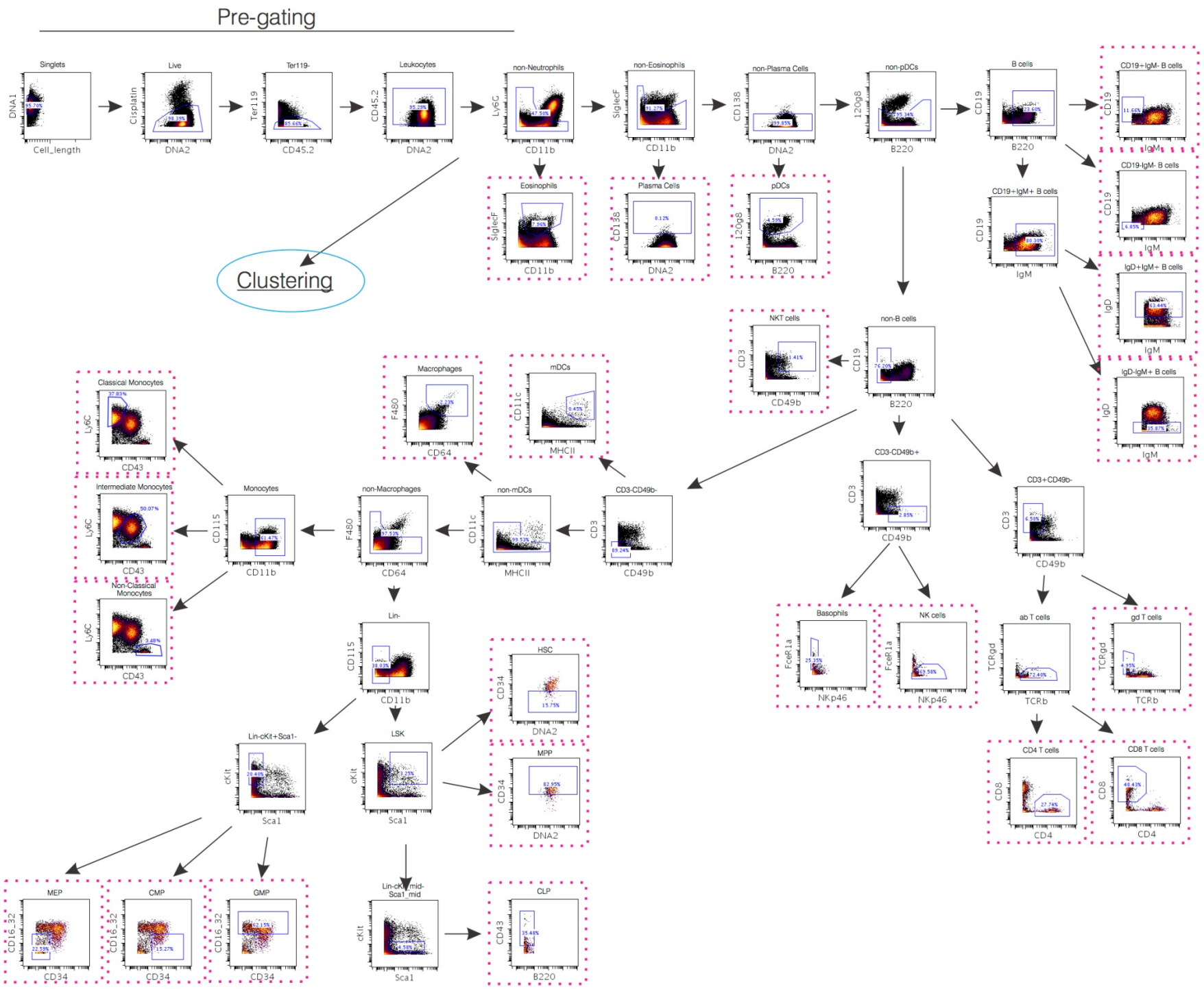

Supporting Figure 2

a

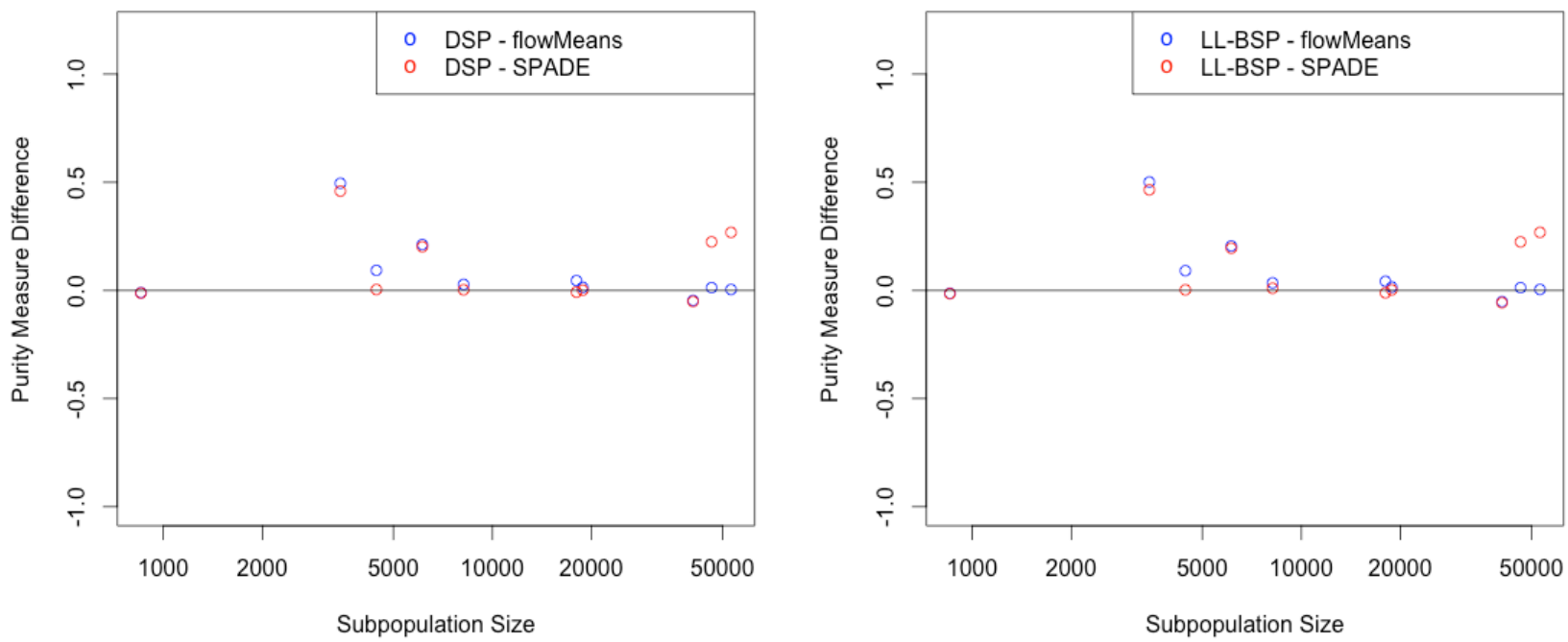

b

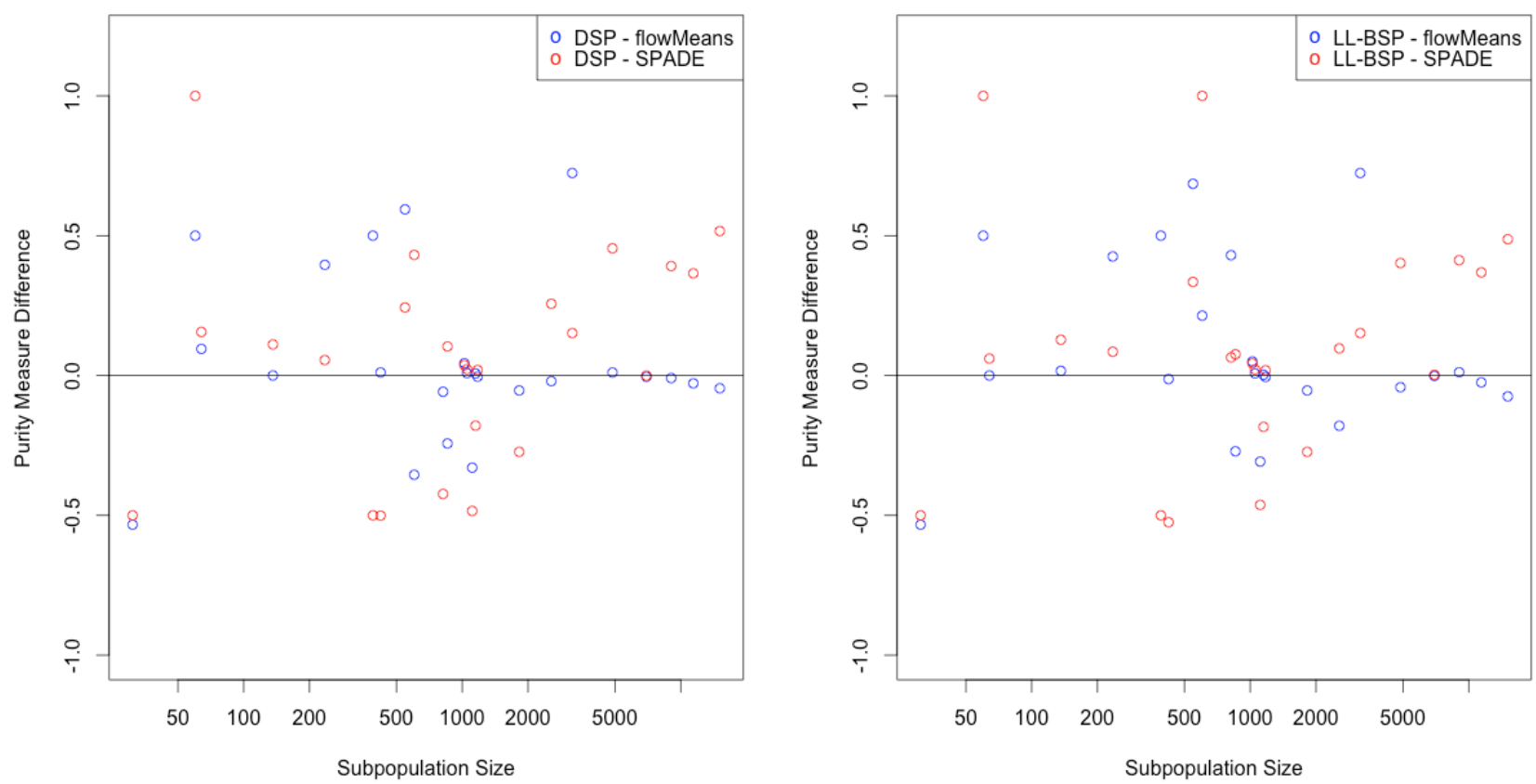

Supporting Figure 3

Sample1

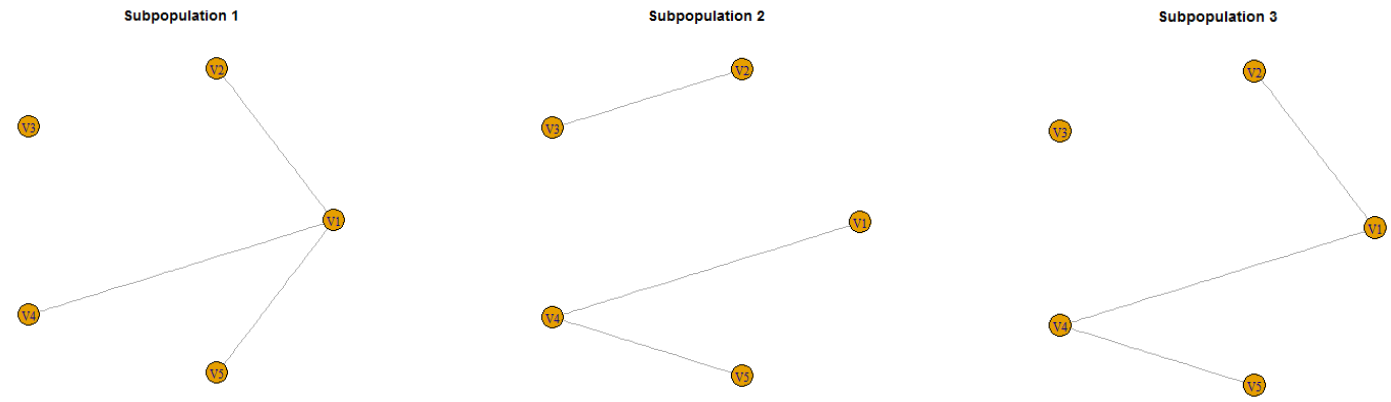

Sample2

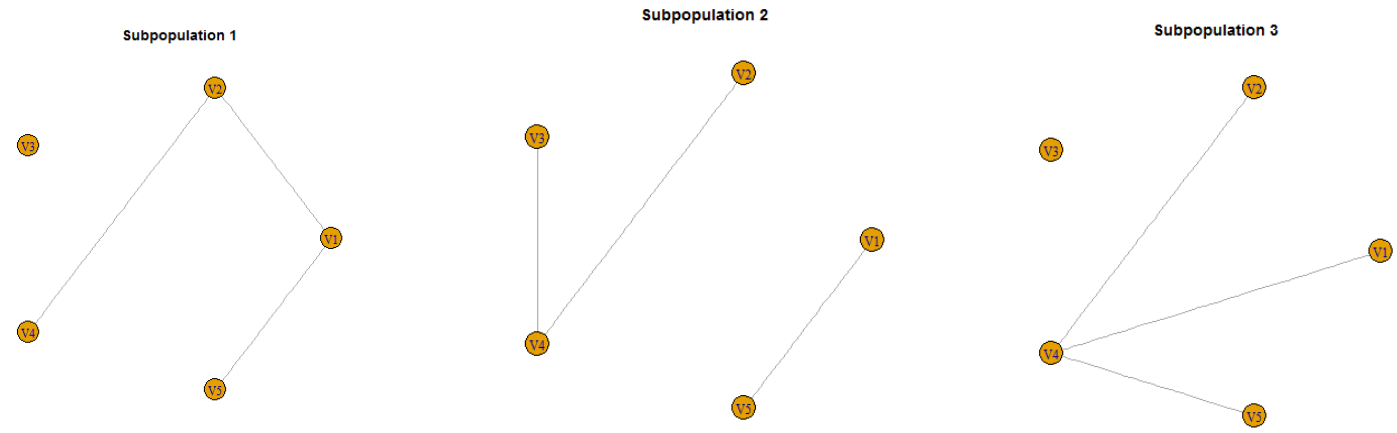

Sample3

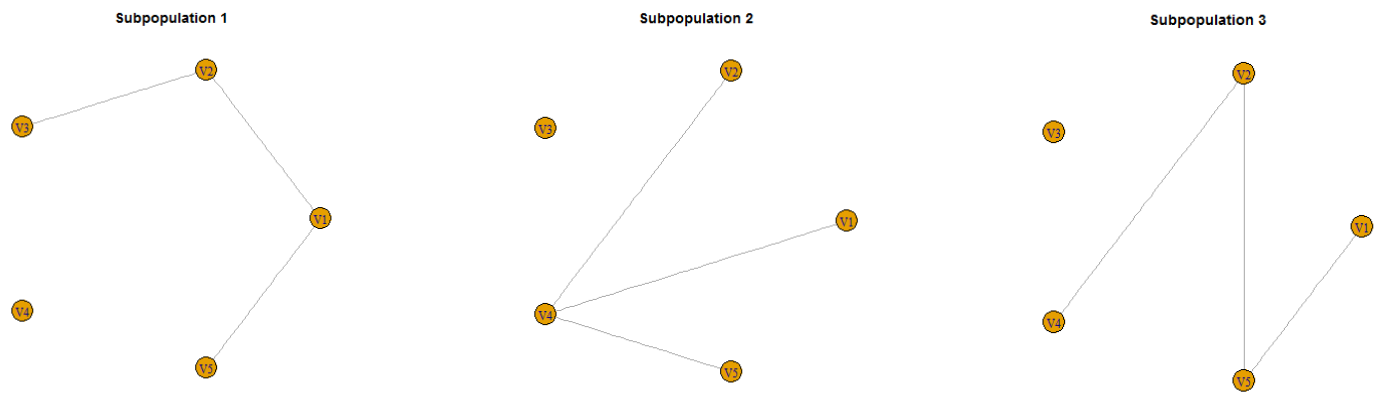

Sample4

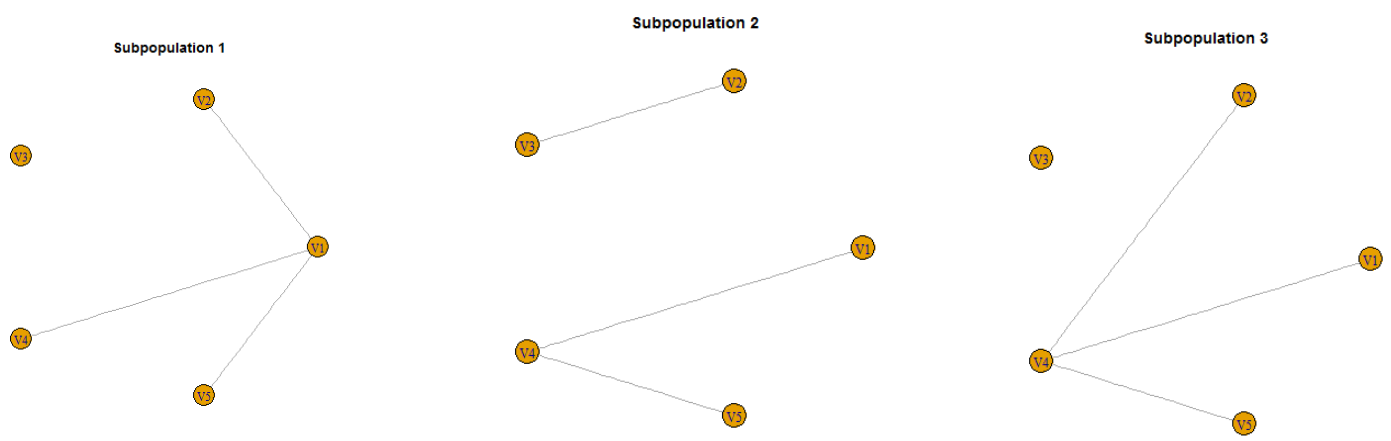

Sample5

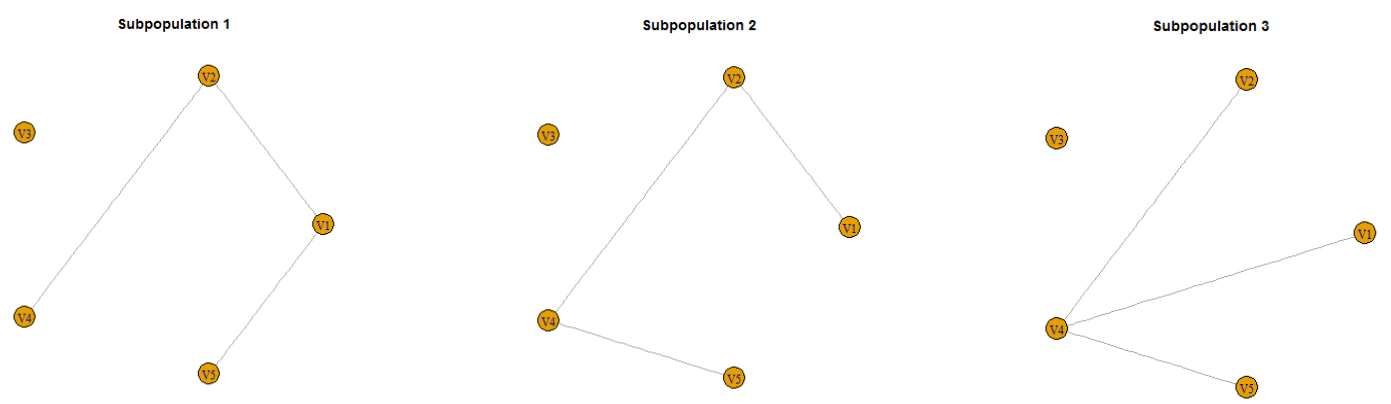

Supporting Figure 4

a

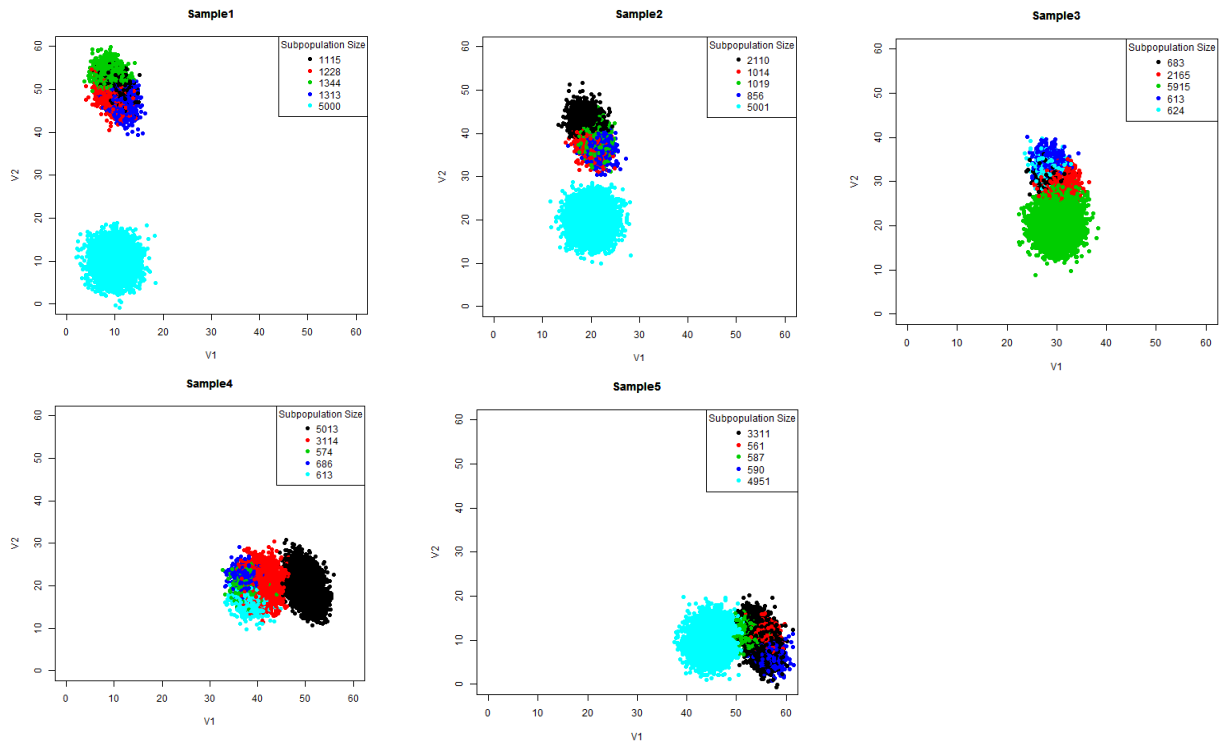

b

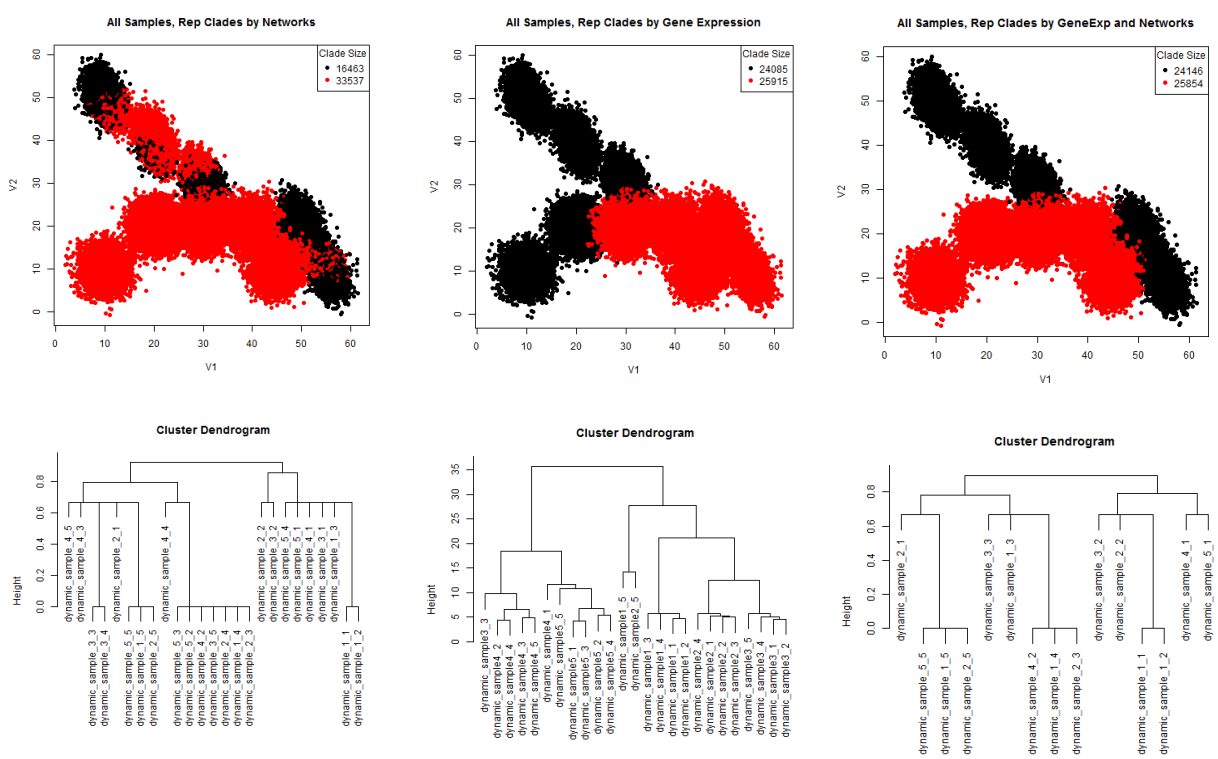

C

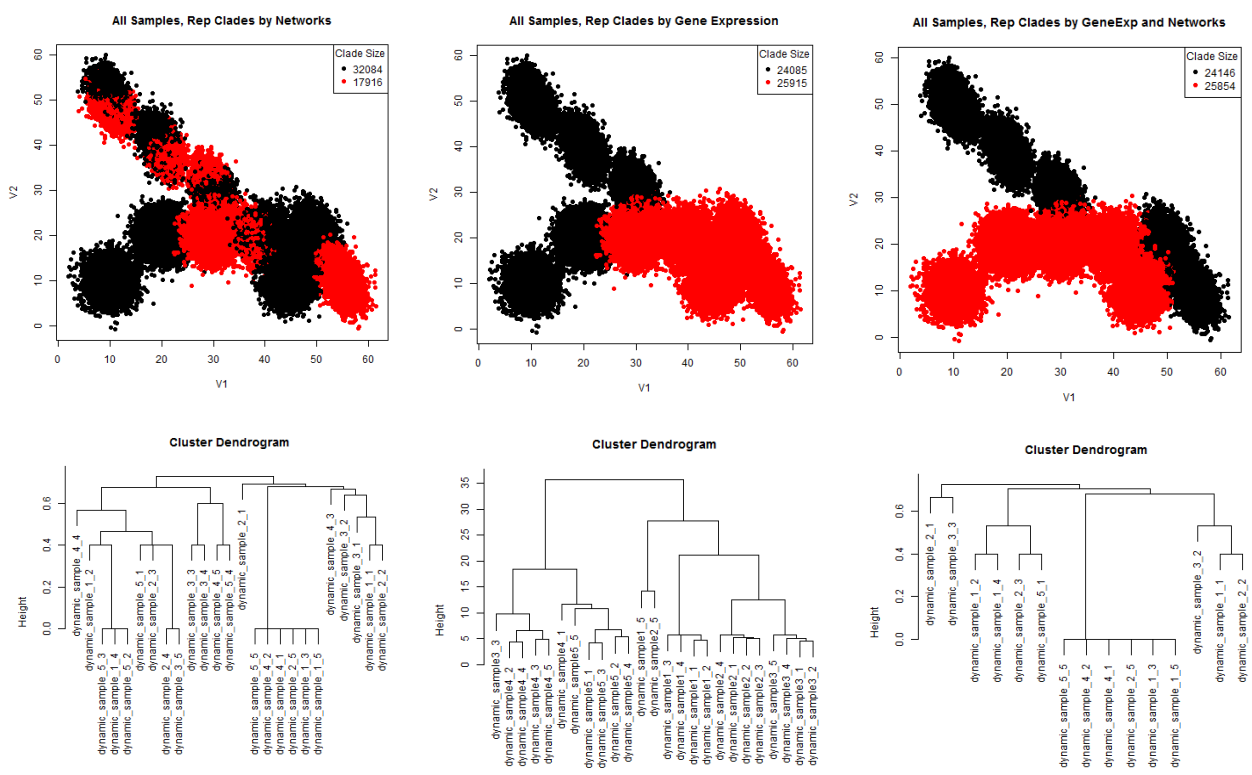

Supporting Figure 5

a

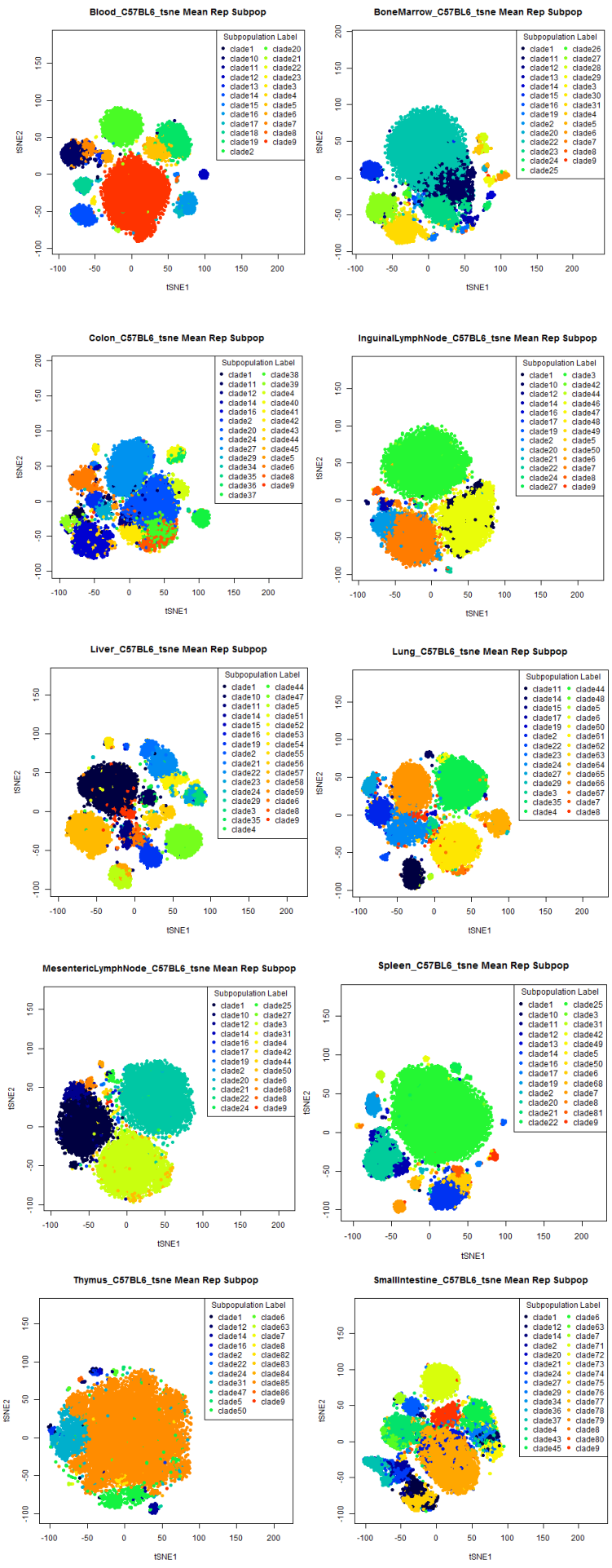

b

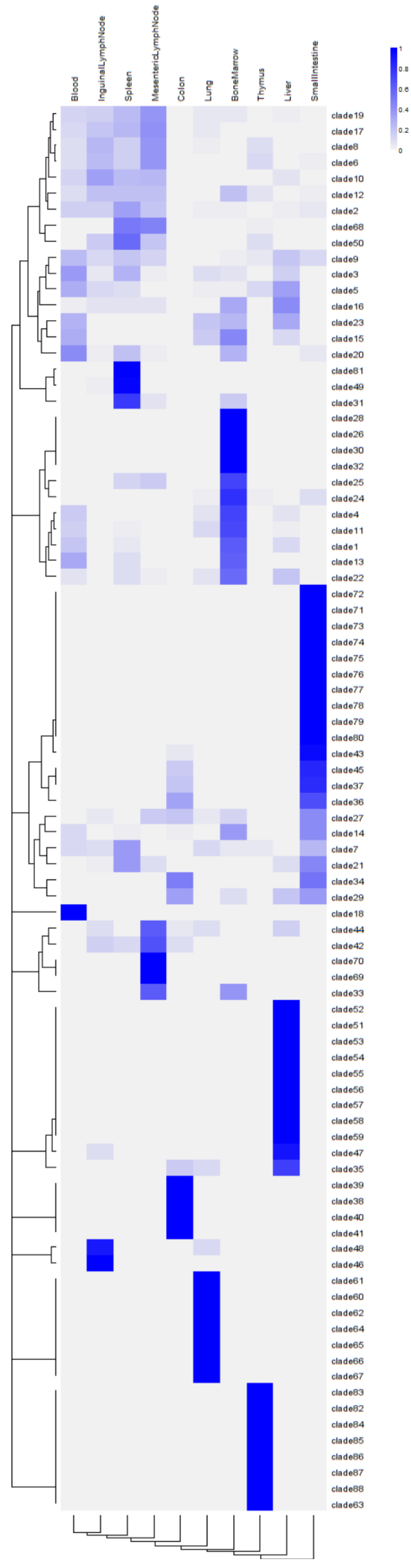

Supporting Figure 6

a

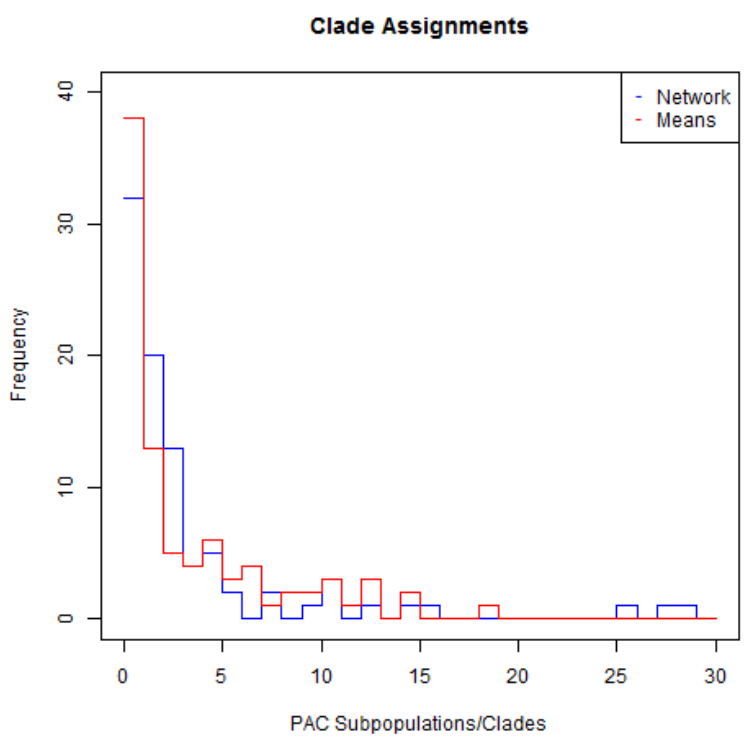

b

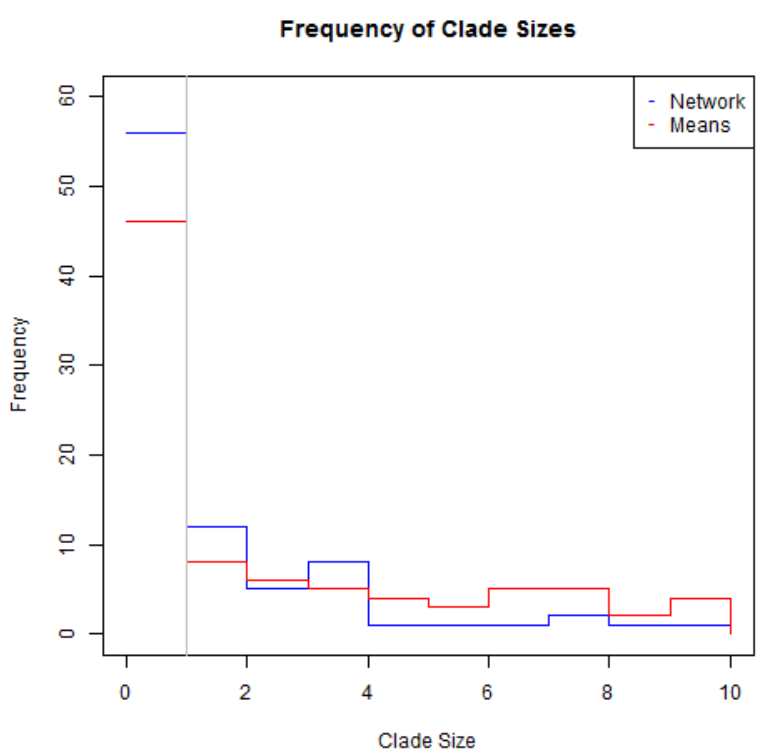

c

Clade	Number of PAC Subpop	p-measure	Dataset-level Proportion	Number of Samples Present
clade3	4	1	1.16726488	4
clade7	5	1	0.826687342	5
clade9	2	1	0.076407462	2
clade15	2	1	0.031185486	2
clade16	5	1	1.283666519	4
clade19	2	1	0.277964818	1
clade22	1	1	0.063776132	1
esc_2_1	1	1	0.000339958	1
esc_2_2	1	1	0.000377731	1
clade32	1	1	0.010417826	1
clade33	3	1	0.216689266	2
clade34	1	1	0.065861208	1
clade39	3	1	0.027634813	1
esc_3_1	1	1	0.001442933	1
clade40	1	1	0.007660388	1
clade43	3	1	0.034947688	1
clade45	2	1	0.043590178	2
clade46	3	1	0.023426888	1
clade47	2	1	0.291140081	2
esc_5_1	1	1	0.004026614	1
clade57	1	1	0.043907472	1
clade60	1	1	0.015026146	1
esc_8_1	1	1	0.000695025	1
clade73	3	1	0.614742379	1
clade74	1	1	0.090496835	1
clade76	1	1	0.008151439	1
esc_10_1	2	1	0.002266387	1
clade80	1	1	0.013688978	1
clade30	4	0.75	0.084717548	3
clade11	15	0.73333	0.645202621	8
clade8	3	0.66667	0.117451732	3
clade28	3	0.66667	0.065249283	2
clade38	3	0.66667	0.052648171	1
clade67	3	0.66667	0.038407706	2
clade1	10	0.5	2.813553327	6
clade10	8	0.5	0.297402864	4
clade13	8	0.5	0.138785989	4
clade17	2	0.5	0.110365495	1
clade18	3	0.5	0.276642759	1
clade24	2	0.5	0.22283873	2
clade41	2	0.5	0.015328331	1
clade54	2	0.5	0.022920728	1
clade55	4	0.5	0.81990329	1
clade62	2	0.5	0.030180721	1
clade6	26	0.42308	24.41300764	9
clade5	29	0.41379	14.76349458	10
clade59	5	0.4	0.030074956	1
clade4	11	0.36364	10.7864008	4
clade14	11	0.36364	0.371619485	4
clade2	28	0.35714	29.79685542	8
clade27	6	0.33333	1.545260467	3
clade37	6	0.33333	0.567828167	2
clade51	3	0.33333	0.174889534	1